Paleoceanography and dinoflagellate cyst record of northwestern North Pacific ODP Site 882 during the Pliocene–Pleistocene transition

Taghi Farmani

Department of Earth Sciences

Submitted in partial fulfillment

of the requirements for the degree of

Master of Science

Faculty of Mathematics and Science, Brock University

St. Catharines, Ontario

Abstract

A palynological study of the Pliocene–Pleistocene transition (2761 to 2497 ka) at Ocean Drilling Program Site 882, located on the Detroit Seamount in the western Subarctic Gyre of the northern North Pacific, provides a detailed record from 68 productive samples of dinoflagellate cysts (dinocysts) and acritarchs with preservation varying from good to moderate. Dinocyst assemblages are characterized by an overwhelming dominance of round brown cysts, scarcity of phototrophs including *Impagidinium* species, and low taxonomic richness (a total of 11 dinocyst taxa for the entire study), reflecting the elevated nutrient levels but harsh conditions and reduced salinities of the North Pacific Subarctic Gyre. Cool, saline surface waters characterize the interval from 2761 to 2.72 Ma, as indicated by relatively abundant *Impagidinium* species including *I. pallidum*. Following the establishment of the modern halocline at ~2.72 Ma, significant shifts are recorded in both dinocyst concentrations and abundances of the acritarch *Cymatiosphaera*? *invaginata*. Productivity evidently remained fairly high even during glacial cycles, including the intense glacial Marine Isotope Stage (MIS) G4 at 2.70 Ma marked by common *Habibacysta tectata* and *Pyxidinopsis reticulata*, implying ice-free conditions at least during the summer. Dinocyst concentrations, and by inference productivity, are at their lowest during MIS 104 (2.6 Ma) which is associated with pronounced cooling in the northern North Atlantic and across the higher latitudes of the Northern Hemisphere. Low abundances of *Cymatiosphaera*? *invaginata* throughout the interval 2600–2565 ka, which includes interglacial MIS 103, unusually suggest reduced precipitation and hence elevated salinities at this time. The interval 2558–2497 ka registers a return to sporadically abundant *Cymatiosphaera*? *invaginata* in glacial MIS 100 and

interglacial MISs 101 and 99, suggesting the return of reduced salinities and perhaps enhanced nutrient levels. In general, productivity seems to remain relatively unchanged although with a peak in interglacial MIS 101. Most species recorded occur within their published stratigraphic ranges. However, this study extends the highest reported occurrence of *Impagidinium detroitense* Zorzi et al., 2020 from Upper Pliocene (2700 ka) to Lower Pleistocene (2544 ka).

Key words: Dinoflagellate, Acritarch, Pacific, Pliocene, Pleistocene

Acknowledgements

I owe a debt of gratitude to Michelle McLean for her financial support when times were rough and passing around was plenty. This thesis would have been left unfinished without her aid. I would like to thank Francine McCarthy for her positive administrative interference in the course of this research at Brock University. The Kochi Core Centre of the International Ocean Discovery Program (IODP) kindly provided the Ocean Drilling Program (ODP) samples used in this study. I am most grateful to Prof. Audrey Limoges (University of New Brunswick) who as external examiner provided many helpful suggestions for the improvement of this thesis. The following are also acknowledged: Profs. Martin J. Head (supervisor), Uwe Brand, and Mike Pisaric, serving as my supervisory committee; and Daksh Patel for his help with laboratory sample processing. This thesis research received support from a Natural Sciences and Engineering Research Council of Canada Discovery Grant to Prof. Martin J. Head, from a Brock University studentship, and from the Faculty of Graduate Studies, Brock University.

Table of contents

List of Figures

List of Tables

List of Acronyms

AOM: amorphous organic matter

DCA: detrended correspondence analysis

DSDP: Deep Sea Drilling Project

IODP: International Ocean Discovery Program

MIS: marine isotope stage

ODP: Ocean Drilling Program

IRD: ice rafted debris

Chapter 1: Introduction

1.1. Pliocene–Pleistocene boundary in the northern North Pacific

The Pliocene–Pleistocene series boundary was re-defined in 2009 using the Monte San Nicola (Sicily) Global boundary Stratotype Section and Point (GSSP) which also defines the base of the Gelasian Stage, Lower Pleistocene Subseries, and Quaternary System (Gibbard and Head, 2010; Head et al., 2021). It has a presently estimated age of 2.58 Ma (Gibbard and Head, 2009). The boundary occurs within a global climate transition that reflects the increasing intensity of Northern Hemisphere glaciation. Key stages in this transition are significant increases in global ice volume during Marine Isotope Stages (MIS) G6–G4 (2.72 Ma), 104 (2.60 Ma), 100 (2.52 Ma), 98 (2.49 Ma), and 96 (2.44 Ma), where the GSSP coincides with the warm MIS 103 (Head et al., 2008). This transition has been studied in the North Atlantic using dinoflagellate cysts that have revealed a major reorganization of surface currents during MIS 104, presumably explained by expanding ice sheets in the Northern Hemisphere at this time (Hennissen et al., 2014; 2015). Pronounced cooling has now been recognised across the Northern Hemisphere at ~2.6 Ma (Hennissen et al., 2015) but not specifically in the northern North Pacific.

Important and influential studies by Haug et al. (1999; 2000; 2015) investigated this transition in the northern North Pacific with a detailed study of Ocean Drilling Program (ODP) Site 882 (50°21’ N, 167°35’ E). This included the establishment of a robust orbitally tuned age model for Site 882. Gaps in our understanding of this transition in the northern North Pacific nonetheless remain. The present study uses dinoflagellate cysts and acritarchs for the first time from this important

site to elucidate more fully changes in paleoceanography and paleoclimate between 2761 and 2497 ka. ODP Site 882 is presently under the influence of the North Pacific Subarctic Gyre and should have recorded ice sheet dynamics in the recent past. Two holes were drilled at this site in August 1992, Hole 882A and Hole 882B (Fig. 1.1). Sedimentation appears continuous and is represented by two lithological subunits, A and B (Rea et al., 1993). Subunit A includes Late Pliocene–Quaternary sediments and is 105 m thick, mostly comprising diatom ooze with calcite. This ooze is generally slightly bioturbated and has burrow fills. Thick ash layers and dropstones are common. Subunit B underlies Subunit A and is of Late Miocene–Pliocene age. This subunit has fewer ash layers and dropstones and is 293.3 m thick (Rea et al., 1993).

Geochemical and microfossil studies of Site 882 revealed the onset of water column stratification in the northwestern North Atlantic at 2.73 Ma in the latest Pliocene, along with the intensification of Northern Hemisphere glaciation. This stratification extended summer sea-surface temperatures well into the fall and provided the required moisture via westerly wind systems that precipitated snow over northern North America (Haug et al., 1999; 2005).

To examine this hypothesis, cored sediments from ODP Site 882 in the northwest North Pacific Ocean have been studied for fossil dinoflagellate cysts (hereafter, “dinocysts”) at high temporal resolution. They allow detailed paleoceanographic reconstructions to be made during the critical 2.8–2.5 Ma interval. This research documents variation within the dinocyst record to elucidate the intense climatic changes and address the moisture supply hypothesis at the scale of individual climate cycles.

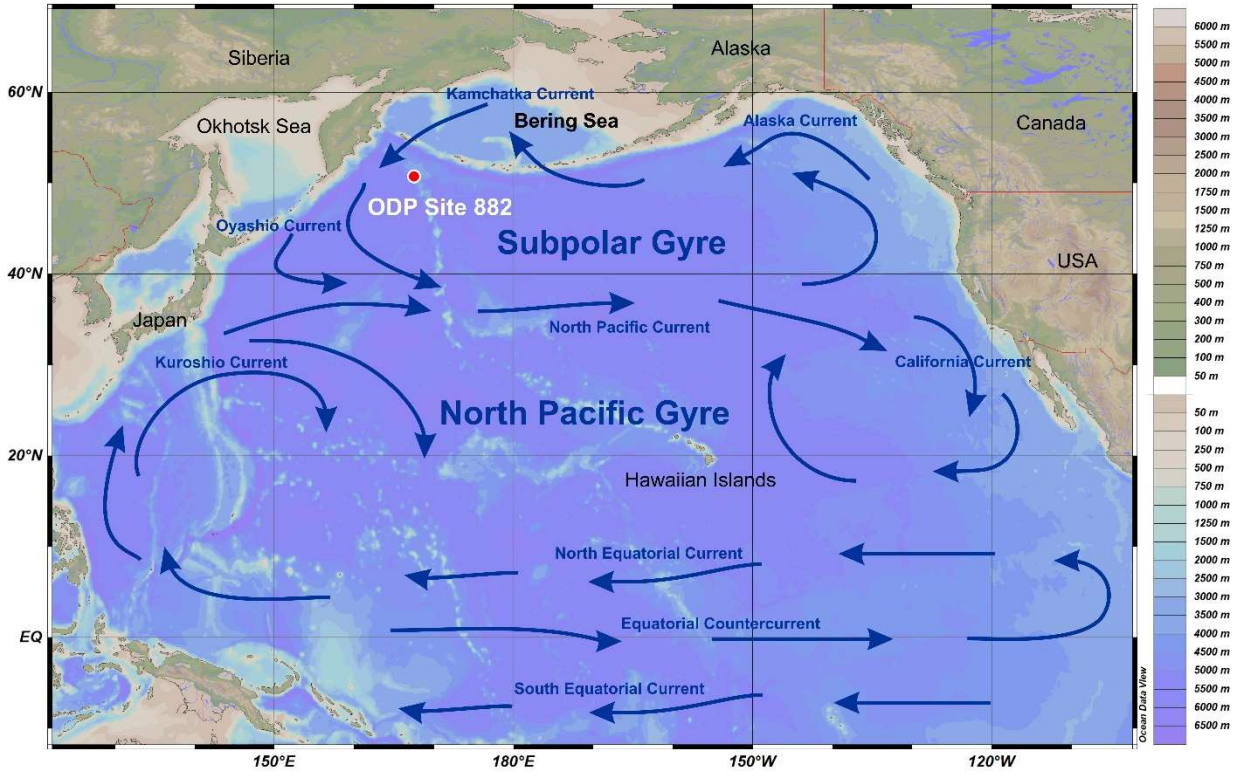

Fig 1.1. North Pacific showing modern surface currents. ODP Site 882 is located in the western part of the Subpolar (or Subarctic) Gyre, also known as the Western Subarctic Gyre. The map was prepared with Ocean Data View software version 5.1.5 (Schlitzer, 2018).

1.2. Dinocysts and their utility for paleoceanographic reconstructions

Dinoflagellates are present in almost all aquatic environments and are among the most important primary producers in the world's oceans. They have a fossil record extending unequivocally to the Late Triassic, and molecular studies suggest an athecate ancestry extending to near the Permian–Triassic boundary (Janouskovec et al., 2016). Dinoflagellates typically have a motile stage within their life cycle, but some also produce a hypnozygotic cyst following sexual fusion

(Stosch, 1973). These resting cysts may have a resistant and distinctively ornamented outer wall. About 13–16% of dinoflagellates produce resting cysts that can be fossilized (Head, 1996). In terms of their nutritional strategy, dinoflagellates may be phototrophs or heterotrophs, and of the phototrophs an increasing number are being revealed as mixotrophic – they ingest prey opportunistically. The cysts of heterotrophic dinoflagellates typically have a brown wall relatively rich in nitrogen (Bogus et al., 2014).

Dinocysts are sensitive to sea-surface conditions and their assemblages reflect changes in the prevailing temperature, salinity, nutrient levels, and in higher latitudes the monthly duration of sea ice. The modern distributions of dinocysts in surface sediments of the seafloor have been studied on a global scale and linked with overlying sea-surface environmental parameters to obtain quantitative information on the autecology of individual species (de Vernal et al., 2020). Using this information, dinocysts are now routinely used in deep ocean cores through the Quaternary to reconstruct past changes in climate and ocean currents (e.g., de Vernal et al., 2001). This makes dinocysts an excellent tool for paleoceanographic studies although they have not been widely utilized for this purpose in the Pacific.

1.3. Oceanography of the North Pacific Ocean

The Subpolar Gyre in the North Pacific Ocean covers the subpolar to polar areas from the northern shorelines of Japan to polar areas of the Bering Sea. The western part of this gyre includes the Kamchatka Current which originates in the western Bering Sea, while the Oyashio

Current flows along the northwestern margin of the northern North Pacific Ocean and close to ODP Site 882 (Fig 1.1). Sea surface temperature (SST) records show that off the cost of California, USA, summer SST reaches as high as 10°C while it reaches as low as 4°C in winter with a uniform salinity throughout the year (Boyer et al., 2013; Kouketsu, 2010).

The southernmost part of the Subpolar Gyre is located around 40° north, where the oceanic currents flow eastward toward the shoreline of the USA. The Subpolar Gyre has a low-salinity surface layer due to high precipitation, with a halocline at the depth of 100 to 120 m (Yuan and Talley, 1996). This low-salinity surface layer extends south to the transition to the North Pacific Gyre at about 40° north (Fig. 1.2).

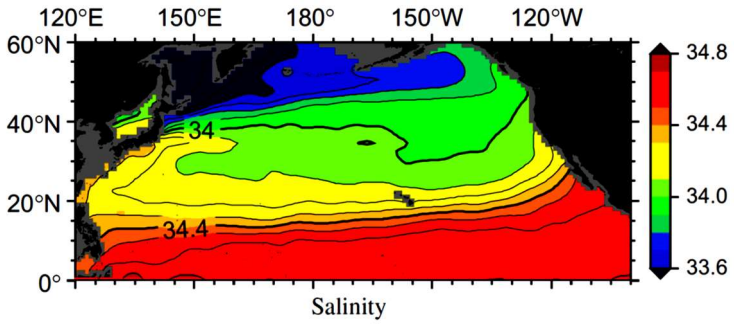

Fig 1.2. Average salinity in the North Pacific Ocean (from Kouketsu et al., 2010). Note that the salinity reaches its lowest value in winter in subarctic areas, where the Subpolar Gyre circulates.

Today, the biological community in the surface waters of the northern Pacific Ocean includes large foraminifera in the spring and smaller ones during the fall. During spring, the photic zone is

dominated by large diatoms and smaller silicoflagellates (Onodera and Takahashi, 2005). In summer, dinoflagellates become abundant with a decrease in other phytoplankton in the mixed layer. This abundance is not due to an increase in nutrients (Mochizoki et al., 2002) but because of reduced competition from diatoms which are more effective in utilizing nutrients. In the fall, there is another bloom of diatoms, but smaller than the bloom in spring (Fig 1.3).

The modern North Pacific Ocean shows highest productivity along the margins of the subarctic gyre, and peak productivity occurs around springtime (Harada et al., 2006). In the northern North Pacific, nutrients are constantly brought to the surface through upwelling currents and vertical mixing, providing the necessary conditions for the growth of microorganisms (Gargett 1991). Research also shows that in subarctic areas of the Pacific Ocean, nutrient levels never reach zero (Chisholm and Morel 1991) despite the presence of a halocline that diminishes vertical mixing (Reid, 1969; Tally, 1993; Warren, 1991). Evidently, silicate-rich deep water is brought to the surface allowing the reproduction of diatoms. The sharp halocline is caused by low-salinity surface waters (Warren 1991, Chisholm and Morel 1991). This stratification in polar and near-polar areas are assumed to have caused a decrease in the rate of CO_2 transfer from ocean to atmosphere (Budyko et al., 1987; Raymo et al., 1996), although a study of carbon isotope records from diatoms through the Upper Pliocene–Lower Pleistocene at Site 882 suggests that stratification did not fundamentally alter CO_2 ventillation to the atmosphere (Swann et al., 2018).

The subpolar areas are rich in nitrite (Lam and Bishop 2008), and iron concentrations are higher in the western Pacific than eastern areas (Nishioka et al., 2007; Zorzi et al., 2019). Modern dinocyst assemblages from the northern North Pacific are characterized by concentrations

ranging from 80 to 682 dinocysts/cm^3 (Bonnet et al., 2012), and are characterized by the dominance of *Nematosphaeropsis labyrinthus*, cysts of *Pentapharsodinium dalei*, *Spiniferites elongatus*, *Islandinium minutum* and round brown cysts (as *Brigantedinium* spp.) (Bonnet et al., 2012).

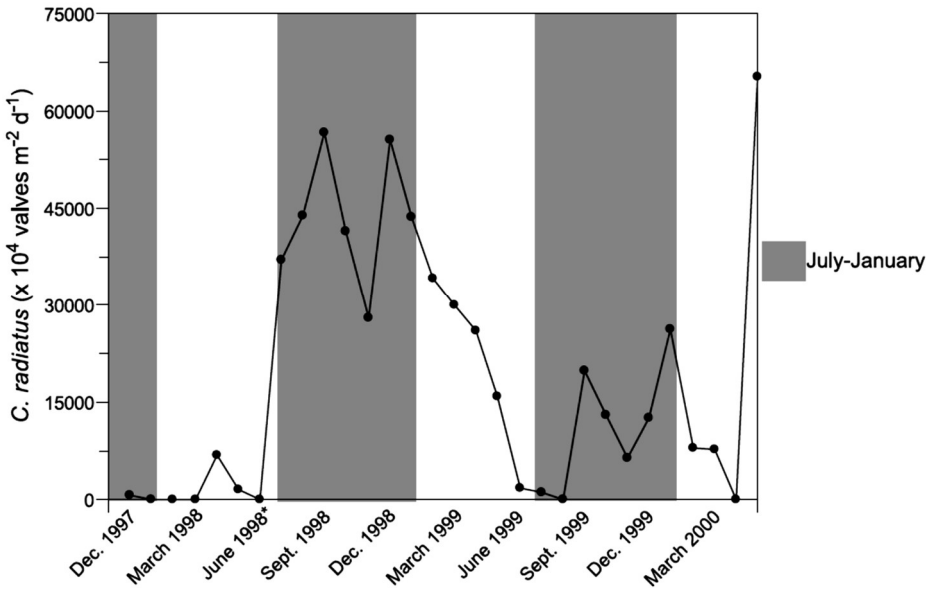

Fig 1.3. Mean monthly fluxes of the diatom *Coscinodiscus radiatus* at station 50°N (50°N, 165°E) in the northwest Subarctic Pacific from December 1997 to May 2000 (from Swann et al., 2006).

1.4. Paleoceanography of the North Pacific Ocean

Present environmental conditions in the North Pacific Ocean, and their effect on marine export productivity, can be traced back to the latest Pliocene. Marine export productivity provides a

mechanism whereby carbon from the atmosphere is transferred to the deep ocean for short-term storage (e.g., glacial to interglacial timescales) or to the sedimentary reservoir for long-term sequestration (e.g., tectonic timescales). Thus, an increase in export production and associated drawdown of atmospheric CO_2 are thought to have mediated climatic cooling during major climate transitions of the Cenozoic (Swann et al., 2006).

The Late Pliocene–Early Pleistocene interval saw a sharp decrease in marine productivity linked to the onset of significant year-round water column stratification (Studer et al., 2012) which has been linked to Northern Hemisphere glaciation (NHG) at 2.73 Ma (Haug et al., 2005; Swann et al., 2006). Stratification caused the surface water to become isolated from the deep water, this stratification persisting today (Swann et al., 2006).

Lithological variations across the northern North Pacific Ocean largely follow 40 kyr ice-volume cycles, with opal-rich deposition occurring during glacial intervals and enhanced carbonate production during interglacials (e.g., Venti and Billups 2012; Venti et al 2017). However, local environmental conditions such as oxidization and the influence of terrestrial input can modify the expression of these global sedimentological cycles.

A key component of northern North Pacific paleoceanography is the production of biogenic opal, which is directly related to the availability of nutrients. It increases when nutrient-rich waters are transferred from depth to the near-surface where diatoms, being photosynthetic, live. At Site 882 in the northwestern North Pacific, the amount of biogenic opal decreased fourfold at 2.73 Ma after which these lower levels were sustained (Haug et al., 1995, 1999, 2005). This abrupt decrease coincides with the pronounced glacial MIS G6 (Fig. 1.4).

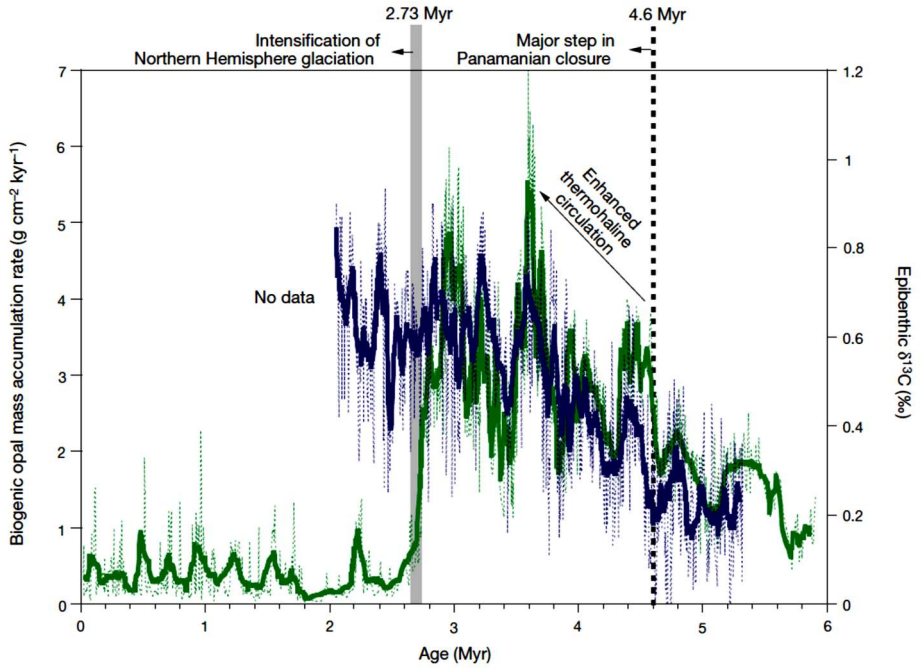

Fig. 1.4. Subarctic Pacific and Caribbean Sea palaeoceanographic records. Shown is a comparison of biogenic opal mass accumulation rates (green line) at ODP Site 882 in the subarctic northwest Pacific and $\delta^{13}C$ values of the epibenthic foraminifer *Cibicidoides wuellerstorfi* (blue line) at ODP Site 999 in the Caribbean Sea (from Haug et al., 1999).

Nutrient levels in the deep water in the Pacific Ocean are controlled by deep ocean circulation. Deep water originates in the North Atlantic and Southern Ocean and becomes enriched as it travels north through the North Pacific Gyre (Broecker and Peng, 1982). This circulation pattern appears to have started around 4.6 Ma and had the effect of decreasing nutrient levels in the Atlantic Ocean and increasing those in North Pacific Ocean (Keir, 1988). This nutrient enrichment resulted in the significant accumulation of opaline silica in sediments of the northern North Pacific prior to the development of the sharp halocline (Haug et al., 1999).

Haug et al. (1995; 1999; 2005; Swann et al., 2006) proposed that the modern halocline in the northern North Pacific, formed at ~2.73 Ma in MIS G6, was caused by excessive precipitation and low evaporation, but may have been triggered by a gradual increase that reached a critical threshold (Haug et al., 1995). In addition to lowered biogenic opal and diatom productivity, a drop in the level of coccolithophore productivity was registered at 2.73 Ma (Studer et al., 2012). All biogeochemical and micropaleontological data confirm that the changes in nutrient levels and halocline across the northern Pacific Ocean initiated at ~2.73 Ma have persisted to the present day (e.g., Haug et al., 1999; 2005; Swann et al., 2006; Studer et al., 2012). This isolation from deeper waters was more intense in late summer causing the sea surface temperature to remain high through fall (Haug et al., 2005). The persistent halocline caused spring blooming diatoms of the genus *Coscinodiscus* to switch at ~2.73 Ma to their present fall–winter growth period (Studer et al., 2012).

Normally, owing to the vertical mixing in the oceans, exchanging carbon and oxygen between atmosphere and ocean occurs continuously regardless of glacial or interglacial climates. However, the development of the halocline in the northern Pacific Ocean may have caused a decrease in the mixing of oceanic–atmospheric carbon, and specifically a reduction in the release of CO_2 to the atmosphere which will have promoted cooling (Haug et al., 2005; Swan et al., 2006). Recent research on Site 882 using diatom carbon isotopes nonetheless suggests that salinity stratification did not fundamentally affect the net ocean–atmosphere flux of CO_2 in the subarctic northwest Pacific Ocean through the latest Pliocene–early Pleistocene (Swann et al., 2018).

1.5. Previous Plio-Pleistocene dinocyst studies of the North Pacific Ocean

The Pacific Ocean has not been studied extensively for dinocysts, unlike the Atlantic Ocean and adjoining seas, with relatively few published studies of their modern distribution and older Quaternary records (reviewed in Balota et al., 2020). There are some reports available for Japanese coastal areas (e.g., Matsuoka et al., 1987; Kurita and Obuse, 2003; and see references in Balota et al., 2021), and sediments younger than 1 million years old (e.g., Miyoshi et al., 1999; Legrand et al., 2021). A recent detailed biostratigraphic analysis published by Balota et al. (2021) across the Lower–Middle Pleistocene boundary at the Chiba composite section in Japan emphasizes the value of dinoflagellate cysts for paleoceanographic reconstruction in the western North Pacific.

Of particular relevance to the present study are reports by Zorzi (2019) and Zorzi et al., (2019; 2020) on the dinocyst record at ODP Site 882 across the Pliocene–Pleistocene transition but at much lower stratigraphic resolution than the present research (4 samples across the interval of our study). According to their research, two common taxa, *Impagidinium pallidum* and *Nematosphaeropsis labyrinthus*, are quite common close to the Plio-Pleistocene boundary with a decrease in salinity after 2.7 Ma due to the formation of the halocline. Zorzi (2019) reports an increase in diversity for samples younger than 1.7 Ma. Other notable studies include Bujak (1984) who examined Eocene–Pleistocene dinocysts from Deep Sea Drilling Project (DSDP) Leg 19 at low stratigraphic resolution but including sites in the Bering Sea and northern North Pacific.

1.6. Aims of the present study

The present research which focuses on the Plio–Pleistocene transition from 2761 ka to 2497 ka seeks to determine the response of dinoflagellates at the scale of individual climate cycles for ODP Site 882. The following specific questions are addressed: What was the response of dinoflagellates to: a) the expansion of Northern Hemisphere ice sheets towards the end of Pliocene at ~2.74 Ma (MIS G6), b) the intense glaciation at the end of the Pliocene (MIS 104, ~2.6 Ma), and c) the first intense glaciation of the Pleistocene (MIS 100, ~1.52 Ma)?

Chapter 2: Study site, materials and methods

2.1. Study location

To understand the changes in dinocyst assemblages across the Pliocene–Pleistocene transition at suborbital resolution, a closely spaced set of samples was acquired. This allows dinoflagellates to be studied in response to climatic, and consequently oceanic changes, over time. Marine isotope stages are based on the $\delta^{18}O$ of benthic foraminiferal tests and reflect, to a degree, global ice volume which allows glacial–interglacial cyclicity to be determined over time. Higher values of $\delta^{18}O$ represent higher levels of global ice volume and by inference colder conditions.

ODP Site 882 is located on the slope of the Detroit Seamount at 3243.8 m below sea level. The primary objective of drilling this site was to obtain high-resolution data of northern North Pacific climate through time. For this purpose, two holes were drilled in 1992: Hole 882A and Hole 882B which are located at 50°21.797'N, 167°35.999'E and 50°21.798'N, 167°35.976'E, respectively (Rea et al. 1993). This study focuses exclusively on the samples obtained from Hole 882A. The Site 882 preliminary report (Rea et al. 1993) classifies the entire lithological profile into two subunits: Subunit IA and Subunit IB.

Subunit IA encompasses the interval between 882A-1H and 882A-12H from the depths of zero to 105 meters below sea floor (mbsf). This subunit is characterized by heavy concentrations of diatom ooze and clay. There are some centimeter-scale burrows in the sediment that indicate slight bioturbation at certain levels. The indication of such activities is also detected in the

palynomorph results (see Results section). This subunit contains 52 ash layers, most of which can be correlated between Holes A and B.

Subunit IB encompasses the interval between 882A-12H and 882A-42H from the depths of 105 to 398.3 mbsf. Diatom ooze is predominant in this subunit as well. The shipboard studies suggests that diatoms constitute between 60% and 100% in this subunit (Rea et al., 1993). Ash layers are less abundant, there being only 17 in total in this subunit. Only six ash layers were recovered from Hole B. The boundary between Subunits A and B as reported by Rea et al. (1993) lies between Samples 12-1, 128–130 cm (2751 ka) and 12-1, 144–146 cm (2752 ka).

The entire interval of drilling at Site 882 is dominated by biogenic silica. High abundances of diatoms are observed until the Lower Pliocene after which they decrease progressively from the Upper Pliocene to Holocene. These changes correlate with increases in the influx of terrigenous sediments (Rea et al., 1993).

2.2. Sedimentation rates

The initial report by Rea et al. (1993) proposed that the average sedimentation rate for Site 882 is 3.8 cm/ky, which was mainly calculated using diatom biostratigraphy datums. Sedimentation rates were later refined as a result of fine orbital tuning of the Site 882 record (Tiedemann and Haug, 1995). Sedimentation rates are at their highest in the lowest part of the studied interval at around 11 cm/kyr, dropping by more than 50% to 5 cm/kyr at ~2.73. They remain at these levels with some fluctuations until ~2.67 ka when they drop to 2 cm/kyr. They rise again to 5 cm/kyr at

2.65 Ma, and then drop to ~2 cm/kyr at 2.62 ka. They remain at low levels of around 2–3 cm/kyr through to the top of the studied interval at 2.50 Ma, with the highest part of this interval (2.53–2.50 Ma) having the lowest sedimentation rates of ~2 kyr (fig. 2 of Tiedemann and Haug, 1995). High sedimentation rates of the latest Pliocene, having dropped sharply at ~2.73 Ma, were never to return. This abrupt decrease in sedimentation rate coincides with the onset of the permanent halocline in the northern North Pacific at ~2.73 Ma in MIS G6 (see Chapters 1 and 5).

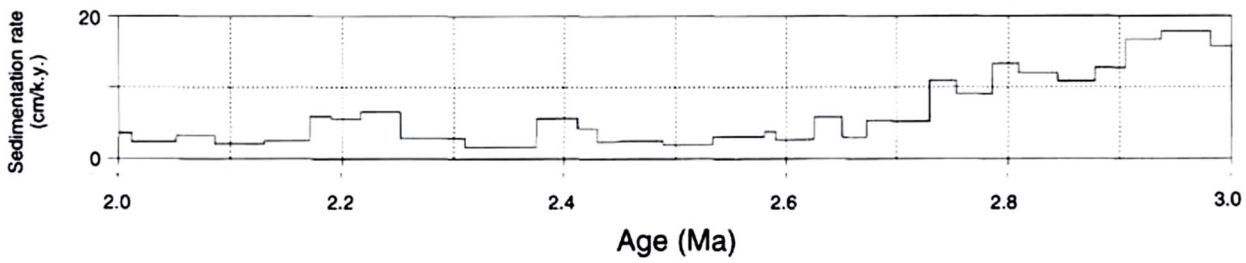

Fig 2.1. Sedimentation rates for Site 882 spanning the duration of the present research (2761 to 2497 ka) based on the fine orbital tuning of sediments (from fig. 2 of Tiedemann and Haug, 1995).

2.3. Methodology

2.3.1. Samples and processing

Seventy-two samples were processed, with an average spacing of 15 cm representing between 1 and 10 thousand years. Samples represent the interval 105.98–94.77 mbsf which is dated at 2.761–2.497 Ma (Table 1, Appendix 2). All samples were dried, weighed, and treated with HCl

and HF following standard procedures used at Brock University (Appendix 3). Between 8 and 17.6 g dry weight of sediment were processed for each sample. One *Lycopodium clavatum* spore tablet (see below) was added to each sample based on the following reasoning. Bonnet et al. (2012) found the average concentration of dinocysts in modern sediments of the western subarctic gyre to be 252/cm^3. To provide efficient and accurate statistical results, it is best that the ratio of cysts per *Lycopodium clavatum* spores is 1:1 (Maher, 1982). Considering the estimated number of dinocysts per cm^3, as well as the average dry weight of samples, one tablet of *L. calavatum* was added to each sample from batch #140119321, which contains 19,855 spores (Table 2.1).

Samples were subjected to 7.2% room-temperature HCl for up to a day, including dilution/neutralization after 9 hours of being introduced to HCl. Samples were then treated with concentrated 40% HF for up to a week, including dilution/neutralization. No hot acids or alkalis were used. Ultrasound was not used because the risk of destroying dinocysts was greater than the benefits of removing amorphous organic matter (AOM).

The residue was sieved at 10 µm, and two to five palynological slides were prepared using glycerine jelly as the mounting medium. A detailed step-by-step account of the palynological preparation procedure is given in Appendix 3. Due to the high abundances of diatoms, some of which were pyritized and thus survived palynological processing, and low abundances of dinocysts, a second preparation made by sieving the remaining unsieved residue was undertaken for many samples. Overall, up to 5 slides were prepared for many samples in order to count up to 300 dinocysts. A total of 179 slides were prepared, among which 128 slides were studied.

Beside dinocysts, other particulate organic matter was also counted, notably acritarchs, pollen, embryophyte spores, fungal spores, foraminiferal test linings, woody debris, and invertebrate remains.

The taxonomy in this study follows De Schepper and Head (2009, 2014), Li et al. (2020), Zorzi et al. (2019, 2020), Van Nieuwenhove et al. (2020), Limoges et al. (2020) and Mertens et al. (2020).

Table 2.1. Samples obtained and studied from ODP Leg 145, Site 882. All samples are from Hole A. Color and reaction to 7.2% room-temperature HCl is given. Some samples received are from slightly different levels than requested due to unavailability of some core intervals.

Core, section, interval (cm)	Depth (mbsf)	Sedimentological observation	No. slides	Lab Label
11-1, 45–47	94.77	Grey to greenish grey/No HCl reaction	2	Tag 1
11-1, 63–65	94.95	Brown in color/No HCl reaction	2	Tag 2
11-1, 84–86	95.16	Grey to greenish grey/No HCl reaction	2	Tag 3
11-1, 101–103	95.33	Grey to greenish grey/No HCl reaction	2	Tag 4
11-1, 114–116	95.46	Grey to greenish grey/No HCl reaction	2	Tag 5
11-1, 128–130	95.60	Grey to greenish grey/No HCl reaction	2	Tag 6
11-1, 146–148	95.78	Grey to greenish grey/No HCl reaction	2	Tag 7
11-2, 4–6	95.86	Greenish grey/No HCl reaction	2	Tag 8
11-2, 21–23	96.03	Grey to greenish grey/No HCl reaction	3	Tag 9
11-2, 44–46	96.26	Grey to greenish grey/No HCl reaction	3	Tag 10
11-2, 62–64	96.44	Grey to greenish grey	2	Tag 11
11-2, 74–76	96.56	Grey to greenish grey/No HCl reaction	2	Tag 12
11-2, 88–90	96.70	Grey to greenish grey/No HCl reaction	2	Tag 13
11-2, 101–103	96.82	Grey to greenish grey/slight reaction	3	Tag 14
11-2, 116–118	96.97	light grey/No HCl reaction	2	Tag 15
11-2, 132–134	97.14	Grey to greenish grey/No HCl reaction	2	Tag 16
11-2, 146–148	97.28	Grey to greenish grey/No HCl reaction	2	Tag 17
11-3, 6–8	97.38	Grey to greenish grey/No HCl reaction	2	Tag 18
11-3, 17–19	97.49	Grey to greenish grey/No HCl reaction	2	Tag 19
11-3, 33–35	97.65	Grey to greenish grey/No HCl reaction	2	Tag 20 (A)

11-3, 42–44	97.74	Grey to greenish grey/No HCl reaction	3	Tag 21
11-3, 62–64	97.94	Grey to greenish grey/No HCl reaction	3	Tag 22
11-3, 86–88	98.18	Grey to greenish grey/No HCl reaction	2	Tag 23
11-3, 103–105	98.35	Grey to greenish grey/No HCl reaction	2	Tag 24
11-3, 118–120	98.50	Grey to greenish grey/No HCl reaction	2	Tag 10
11-3, 134–136	98.66	Grey to greenish grey/No HCl reaction	3	Tag 20 (B)
11-4, 0–2	98.82	Grey to greenish grey/No HCl reaction	3	Tag 30
11-4, 7–9	98.89	Grey to greenish grey/No HCl reaction	2	Tag 40
11-4, 33–35	99.15	Grey to greenish grey/No HCl reaction	2	Tag 50
11-4, 52–54	99.34	Grey to greenish grey/No HCl reaction	2	Tag 60
11-4, 63–65	99.45	Grey to greenish grey/No HCl reaction	2	Tag 70
11-4, 82–84	99.64	Grey to greenish grey/No HCl reaction	2	Tag 80
11-4, 104–106	99.86	Grey to greenish grey/No HCl reaction	2	Tag 90
11-4, 122–124	100.04	Grey to greenish grey/No HCl reaction	2	Tag 100
11-4, 144–146	100.26	Grey to greenish grey/No HCl reaction	2	Tag 110
11-5, 2–4	100.34	Grey to greenish grey/No HCl reaction	2	Tag 120
11-5, 22–24	100.54	Light Grey/Slight reaction	2	Tag 130
11-5, 36–38	100.68	Grey to greenish grey/No HCl reaction	2	Tag 140
11-5, 47–49	100.79	Grey to greenish grey/No HCl reaction	2	Tag 150
11-5, 67–69	100.99	Greenish grey/Slight reaction	2	Tag 160
11-5, 91–93	101.23	Grey to greenish grey/No HCl reaction	2	Tag 170
11-5, 114–116	101.46	Grey to greenish grey/No HCl reaction	2	Tag 180
11-5, 132–134	101.64	Grey to greenish grey/No HCl reaction	3	Tag 190
11-5, 146–148	101.78	Grey to greenish grey/No HCl reaction	2	Tag 200
11-6, 4–6	101.86	Grey to greenish grey/No HCl reaction	2	Tag 210
11-6, 22–24	102.04	Grey to greenish grey/No HCl reaction	2	Tag 220
11-6, 35–37	1102.17	Grey to greenish grey/No HCl reaction	2	Tag 230
11-6, 54–54	102.36	Grey to greenish grey/No HCl reaction	2	Tag 240
11-6, 67–69	102.49	Grey to greenish grey/No HCl reaction	3	DP 1
11-6, 97–99	102.79	Grey to greenish grey/No HCl reaction	3	DP 2
11-6, 112–114	102.94	Grey to greenish grey/No HCl reaction	2	DP 3
11-6, 125–127	103.07	Grey to greenish grey/No HCl reaction	3	DP 4
11-6, 142–144	103.24	Grey to greenish grey/No HCl reaction	3	DP 5
11-7, 6–8	103.38	Grey to greenish grey/No HCl reaction	3	DP 6
11-7, 23–25	103.55	Grey to greenish grey/No HCl reaction	3	DP 7
11-7, 46–48	103.78	Grey to greenish grey/No HCl reaction	3	DP 8
11-7, 61–63	103.93	Grey to greenish grey/No HCl reaction	3	DP 9
12-1, 0–2	103.95	Grey to greenish grey/No HCl reaction	3	DP 10
12-1, 16–18	103.98	Grey to brown/No HCl reaction	3	DP 11
12-1, 32–34	104.14	Grey to brown/No HCl reaction	3	DP 12
12-1, 48–50	104.30	Grey to greenish grey/No HCl reaction	4	DP 13

12-1, 64–66	104.46	Grey to greenish grey/No HCl reaction	3	DP 14
12-1, 77–79	104.59	Grey to greenish grey/No HCl reaction	5	DP 15
12-1, 96–98	104.78	Grey to greenish grey/No HCl reaction	4	DP 16
12-1, 112–114	104.94	Grey to greenish grey/No HCl reaction	4	DP 17
12-1, 128–130	104.10	Grey to greenish grey/No HCl reaction	3	DP 18
12-1, 144–146	105.26	Grey to greenish grey/No HCl reaction	3	DP 19
12-2, 2–4	105.34	Grey to greenish grey/No HCl reaction	4	DP 20
12-2, 18–20	105.50	Grey to greenish grey/No HCl reaction	3	DP 21
12-2, 34–36	105.66	Grey to greenish grey/No HCl reaction	3	DP 22
12-2, 51–53	105.83	Grey to greenish grey/No HCl reaction	3	DP 23
12-2, 66–68	105.98	Grey to greenish grey/No HCl reaction	3	DP 24

2.3.2. Statistical analyses

The following statistical analyses were conducted for this research.

2.3.2.1. Calculation of absolute numbers of dinocysts

Based on the introduction of *L. clavatum* spores, the estimations of absolute numbers of dinocysts per gram dry weight was calculated following Stockmarr (1971). The absolute numbers of dinocysts are reported in Chapter 4. This parameter can generate a visual graph, which makes tracking the changes in inferred productivity over time clearer. The productivity of the surface water and its changes over time are discussed in Chapter 5.

2.3.2.2. Constrained cluster analysis

Constrained cluster analysis was performed with the help of PAST software version 4.04 (Hammer et al., 2021) to visualize objectively the changes in dinocyst assemblages through time. The analyses utilize stratigraphic constraint and a paired group algorithm with the Gower

similarity index. Results showing the clustering of dinocyst assemblages in stratigraphic order are presented in Chapter 4.

2.3.2.3. Detrended correspondence analysis

Modeling species based on their respective abundances follows the assumption that each species becomes more abundant as the limiting environmental factors decrease: it disperses in ways that exploit favourable conditions as best as possible. Detrended correspondence analysis (DCA) models species according to the limiting conditions of their environment. For dinoflagellates, these conditions are mostly temperature, salinity, and nutrient levels (Dale and Dale, 2002). DCA calculates scores for both species and samples. All counted particulate organic matter, including acritarchs and terrestrial organic material, were entered on a spreadsheet in PAST software 4.04 (Hammer et al., 2001). The plot for both samples and species was generated using DCA ordination with 26 segments. The segments and the axis properties can be finely adjusted for improved visualization. DCA for the ODP Site 882 data set for all particulate matter (this study) is presented in Chapter 4.

2.3.2.4. Relative abundance of *Cymatiosphaera*? *invaginata*

The relative abundance of *Cymatiosphaera*? *invaginata* was calculated in this study to track changes in water-mass characteristics using the following formula: *C.*? *invaginata* / (total dinocysts + *C.*? *invaginata*) x 100.

2.3.2.5. Dinocyst transfer functions

Transfer functions using the modern analog approach allow the quantitative reconstruction of hydrographic parameters (sea-surface temperature, salinity, nutrient levels, duration of sea ice) for each fossil assemblage by comparing that assemblage with one or more modern (surface sediment) assemblages for which the hydrographic parameters are already known (de Vernal et al., 2001; 2021). It requires an adequate coverage of modern assemblages – the calibration set. A detailed modern calibration set is not available for the North Pacific (Balota et al., 2021) and accordingly transfer functions were not used in the present study. Moreover, important inferences can be made using often high abundances of the acritarch *Cymatiosphaera*? *invaginata* which is neither a dinoflagellate nor extant.

Chapter 3: Age of studied interval

3.1. Age model

The ages of samples used for the present study are based on the age model of Tiedemann and Haug (1995). It is not possible to use foraminiferal $\delta^{18}O$ measurements at this subarctic site because of the discontinuous record of carbonate. These authors instead used the GRAPE (gamma-ray attenuation porosity evaluation) sediment density record on the core which, from time series analysis, revealed a strong signal in the precession bandwidth. At Site 882, the GRAPE record reflects density differences resulting from fluctuations in the deposition of biogenic opal and ice-rafted debris (IRD), and in both the deposition and dissolution of carbonate (Tiedemann and Haug, 1995).

The GRAPE record was tuned to summer insolation at 65°N back to 4 Ma using the solution of Berger and Loutre (1991). Independent tie points are provided by paleomagnetic reversals. The error in the ages is a few thousand years based on the unknown delay of the GRAPE record relative to the astronomical tuning target. Magnetic susceptibility at Site 882 is also very sensitive to orbital forcing, particularly because of the influence on IRD. However, the GRAPE record was found to be more sensitive to precession, and was also more sensitive in the earlier part of the Pliocene where IRD is not present.

Tiedemann and Haug (1995) mostly used the precession signal for tuning, but where this was weakly expressed (e.g. 2.58–2.45 Ma and 1.95–1.77 Ma) they used the obliquity response. In general, there was strong coherence between the precession and obliquity signals especially

between 1 and 3.6 Ma. The age model resulted in high levels of IRD in MIS 96–100, 104, and G6 which is highly plausible.

Tiedemann and Haug (1995; Table 3.1) gave age control points for their tuned model, and Haug and Sarnthein (2005) provided a detailed record of biogenic silica (%) that used the Tiedemann and Haug (1995) age model. The present study uses Haug and Sarnthein (2005) to assign ages to the samples analyzed. Where a sample interval is not provided by Haug and Sarnthein (2005), its age is interpolated from the closest samples listed. Ages of samples used in the present study are given in Table 3.2 and range from 2761 to 2497 ka.

As noted above, a continuous foraminiferal isotope record is not available for Site 882. However, in order to visualize the marine isotope stages against the Site 882 records, the benthic $\delta^{18}O$ records from ODP Sites 849 by Jakob et al. (2017) (Equatorial East Pacific Rise) and 846 by Haug and Sarnthein (2005) (Equatorial East Pacific south of the Galapagos Islands) are transposed alongside them (Fig. 3.1).

The initial report from ODP Site 882 presents a good correlation between magnetic susceptibility and the changes in oxygen isotopes. According to the measurements of Rea et al. (1993), magnetic susceptibility increases in warmer stages such as MIS 101 and 103 due to the increase in fine material resulting from ice rafted debris. The magnetic susceptibility curve can in fact be correlated visually with LR04 stack. However, for better comparison between sites, the magnetic susceptibility is compared with oxygen isotope data provided from ODP Sites 846 and 849 (Fig 3.1. C, D).

The magnetic susceptibility curve suggests that the amount of ice rafted debris is much greater for the Pleistocene than the Pliocene. It appears that the amount of fine material resulted from the melting ice decreases almost by half, even in warm isotopic stages of the Pliocene. However, the peaks in magnetic susceptibility correlate well with the peak of warm intervals recorded throughout the selected study range (i.e., MIS 99, 101, 103, G1, G3, G5, G7).

GRAPE values as measured and reported by Rea et al. (1993) reflect the amount of biogenic opal, with an increase in values associated with the increase of biogenic opal (Studer et al., 2012). Visual correlation shows GRAPE values positively correlated with magnetic susceptibility, both showing peaks at interglacial isotope stages.

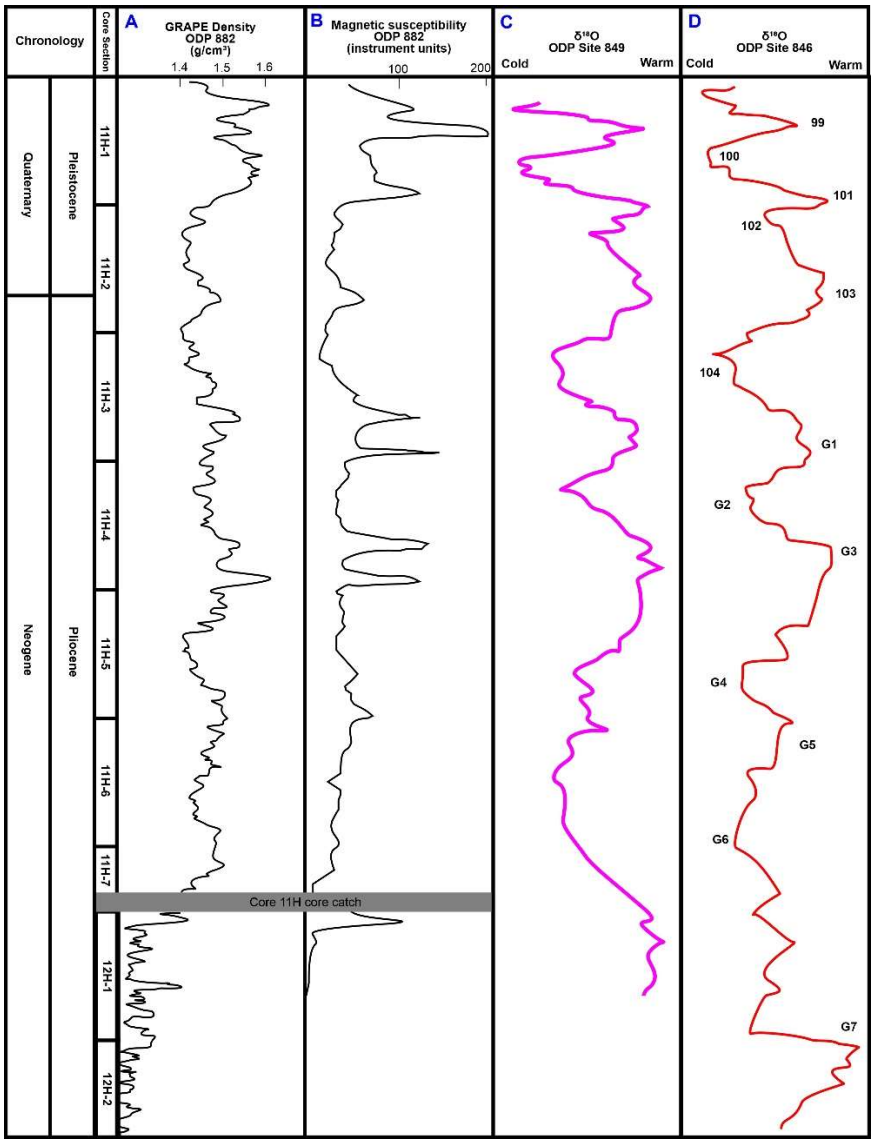

Fig 3.1. Graphical correlation of age models from ODP Sites 849 (Equatorial East Pacific Rise) and 846 (Equatorial East Pacific south of the Galapagos Islands) with ODP Site 882. **A and B.** The GRAPE density and magnetic susceptibility of Hole 882A is from Rea et al. (1993). **C**. Benthic foraminiferal oxygen isotope values (*C. wuellerstorfi*) from ODP Site 849 reported and tuned to the LR04 age model of Lisieki and Raymo (2005) and calibrated by Jakob et al. (2017). **D**. Benthic foraminiferal oxygen isotope values from ODP Site 846 with marine isotope stages labelled (Haug and Sarnthein, 2005).

3.2. Age of samples

Initial research on ODP Site 882 (Tiedemann and Haug, 1995) provides orbitally tuned ages for 36 samples within the selected interval of the present study. Other studies have since used this age model for ODP Site 882 (e.g., Galbraith et al., 2007; Jaccard et al., 2009; Martinez-Garcia et al., 2010; Bailey et al., 2011).

The ages of samples for the present study were calculated by linear interpolation using the 36 samples of Tiedemann and Haug (1995) and subsequently Haug and Sarnthein (2005; Table 3.1). The dataset of Haug and Sarnthein (2005) for biogenic silica is available for download from: https://doi.pangaea.de/10.1594/PANGAEA.315090 for both Hole 882A and 882B. The ages of samples from Hole 882A, Core 11H and 12H can be found in Table 3.2.

Table 3.1. The ages of samples from Tiedemann and Haug (1995) used by Haug and Sarnthein (2005) for ODP Hole 882A, Core 11H and 12H. This is part of the dataset from Haug and Sarnthein (2005). These samples and their age were used to interpolate the age of samples for this study.

Leg, hole, core, section, interval (cm)	Depth (m)	Age (ka)
145-882A-11H-1, 80–84	95.12	2516
145-882A-11H-1, 104–108	95.36	2528
145-882A-11H-1, 140–144	95.72	2542
145-882A-11H-2, 20–24	96.02	2551
145-882A-11H-2, 50–54	96.32	2561
145-882A-11H-2, 80–84	96.62	2570
145-882A-11H-2, 104–108	96.86	2578

145-882A-11H-2, 140–144	97.22	2587
145-882A-11H-3, 20–24	97.52	2597
145-882A-11H-3, 50–54	97.82	2608
145-882A-11H-3, 80–84	98.12	2619
145-882A-11H-3, 104–108	98.36	2626
145-882A-11H-3, 140–144	98.72	2632
145-882A-11H-4, 20–24	99.02	2637
145-882A-11H-4, 50–54	99.32	2642
145-882A-11H-4, 80–84	99.62	2647
145-882A-11H-4, 104–108	99.86	2653
145-882A-11H-4, 142–146	100.24	2665
145-882A-11H-5, 20–24	100.52	2673
145-882A-11H-5, 50–54	100.82	2679
145-882A-11H-5, 80–84	101.12	2684
145-882A-11H-5, 104–108	101.36	2689
145-882A-11H-5, 140–144	101.72	2695
145-882A-11H-6, 20–24	102.02	2701
145-882A-11H-6, 50–54	102.32	2707
145-882A-11H-6, 80–84	102.62	2712
145-882A-11H-6, 104–108	102.86	2717
145-882A-11H-6, 140–144	103.22	2724
145-882A-11H-7, 20–24	103.52	2729
145-882A-12H-1, 50–54	104.32	2745
145-882A-12H-1, 80–84	104.62	2748
145-882A-12H-1, 104–108	104.86	2750
145-882A-12H-1, 140–144	105.22	2753
145-882A-12H-2, 19–23	105.51	2756
145-882A-12H-2, 50–54	105.82	2759
145-882A-12H-2, 80–84	106.12	2762

The intervals involved are usually not more than 30 cm in depth, which makes the interpolation fairly accurate. There is, however, a relatively large gap between Samples 11H-7, 20–24 cm and 12H-1, 50–54 cm representing 2729–2745 ka, which marks an interval of about 14 ky. The present study has six samples from this interval. Even though these samples are dated with lower

certainty, the higher sedimentation rate at this interval reduces the error both in depth and age (see section 2.2. Sedimentation rate).

The youngest sample chosen for this study is Sample 882A-11H-1, 50–52 cm, which corresponds to 2497 ka. The oldest sample chosen is Sample 882A-12H-2, 70–72 cm, which corresponds to 2761 ka. This time interval encompasses the major events in the Pliocene and Pleistocene, including the intensification of Northern Hemisphere glaciation at 2.73 Ma and the Pliocene–Pleistocene boundary at 2.58 Ma.

Table 3.2. Ages of samples processed from ODP Hole 882A. Ages are interpolated from the orbitally tuned age model of Tiedemann and Haug (1995) and Haug and Sarnthein (2005).

Processed samples: core/section/interval (in cm)	Depth (m)	Age (ka)	MIS Peak
11-1, 45–47	94.77	2497	98 (cold)
11-1, 63–65	94.95	2506	
11-1, 84–86	95.16	2517	99 (warm)
11-1, 101–103	95.33	2519	
11-1, 114–116	95.46	2521	
11-1, 128–130	95.60	2532	100 (cold)
11-1, 146–148	95.78	2544	
11-2, 4–6	95.86	2548	101 (warm)
11-2, 21–23	96.03	2551	
11-2, 44–46	96.26	2558	
11-2, 62–64	96.44	2565	102 (cold)
11-2, 74–76	96.56	2570	
11-2, 88–90	96.70	2574	
11-2, 101–103	96.82	2577	
11-2, 116–118	96.97	2580	103 (warm)
11-2, 132–134	97.14	2585	
11-2, 146–148	97.28	2589	
11-3, 6–8	97.38	2593	

11-3, 17–19	97.49	2596	
11-3, 33–35	97.65	2601	104 (cold)
11-3, 42–44	97.74	2605	
11-3, 62–64	97.94	2612	
11-3, 86–88	98.18	2620	
11-3, 103–105	98.35	2624	
11-3, 118–120	98.50	2628	
11-3, 134–136	98.66	2631	G1 (warm)
11-4, 0–2	98.82	2633	
11-4, 7–9	98.89	2635	
11-4, 33–35	99.15	2639	
11-4, 52–54	99.34	2642	
11-4, 63–65	99.45	2644	
11-4, 82–84	99.64	2648	G2 (cold)
11-4, 104–106	99.86	2652	
11-4, 122–124	100.04	2659	
11-4, 144–146	100.26	2665	
11-5, 2–4	100.34	2669	
11-5, 22–24	100.54	2673	G3 (warm)
11-5, 36–38	100.68	2676	
11-5, 47–49	100.79	2678	
11-5, 67–69	100.99	2682	
11-5, 91–93	101.23	2686	
11-5, 114–116	101.46	2690	G4 (cold)
11-5, 132–134	101.64	2694	
11-5, 146–148	101.78	2696	
11-6, 4–6	101.86	2698	
11-6, 22–24	102.04	2701	G5 (warm)
11-6, 35–37	102.17	2703	
11-6, 54–54	102.36	2706	
11-6, 67–69	102.49	2710	
11-6, 97–99	102.79	2715	
11-6, 112–114	102.94	2718	
11-6, 125–127	103.07	2720	
11-6, 142–144	103.24	2721	G6 (cold)
11-7, 6–8	103.38	2726	
11-7, 23–25	103.55	2730	
11-7, 46–48	103.78	2731	
11-7, 61–63	103.93	2732	
12-1, 0–2	103.95	2736	
12-1, 16–18	103.98	2741	G7 (warm)

12-1, 32–34	104.14	2743	
12-1, 48–50	104.30	2744	
12-1, 64–66	104.46	2746	
12-1, 77–79	104.59	2747	
12-1, 96–98	104.78	2749	
12-1, 112–114	104.94	2750	
12-1, 128–130	105.10	2751	
12-1, 144–146	105.26	2752	
12-2, 2–4	105.34	2753	G8 (cold)
12-2, 18–20	105.50	2756	
12-2, 34–36	105.66	2757	
12-2, 51–53	105.83	2759	
12-2, 66–68	105.98	2761	

Chapter 4: Results

In total 72 samples were studied. The dinocyst record shows relatively low diversity throughout and is dominated by round brown cysts (including *Brigantedinium* spp.) which constitute the heterotrophic component. The phototrophic dinocysts are represented by *Nematosphaeropsis labyrinthus*, *Impagidinium detroitense*, *I. aculeatum, I. pallidum, I. patulum, Habibacysta tectata*, and *Pyxidinopsis reticulata*. In addition to dinocysts, the acritarchs *Cymatiosphaera*? *invaginata* and *Cymatiosphaera* sp. 1 are present, with the former often abundant, and the chlorophyte *Tasmanites* sp. also present in low abundances throughout.

Terrestrial particulate organic matter in the present study mostly comprises woody debris, pollen, and spores. There is also an abundance of invertebrate remains, possibly related to copepods, throughout this study. The distributions of taxa recorded in the present study are shown in Figs. 4.1 and 4.2 and most are illustrated in Appendix 1. The raw counts are given in Appendix 2.

All but four samples yielded palynomorphs. The four unproductive samples mainly contain AOM and a precipitate which presumably diluted and obscured whatever palynomorphs were present. These samples are 11-5, 132–134 cm (2694 ka, 101.64 m), 11-3, 62–64 cm (2612 ka, 97.94 m), 11-3, 42–44 cm (2605 ka, 97.74 m), and 11-1, 61–63 cm (2506 ka, 94.95 m). They are not shown on Figs. 4.1 and 4.2.

4.1. Marine Palynomorph Assemblage Biozones and Constrained Cluster Analysis

The dinocyst and marine acritarch record is subdivided into four informal assemblage biozones, Biozones 1–4, of which Biozone 4 is divided into sub-biozones 4A and 4B. These biozones and sub-biozones are shown in Figs. 4.1 and 4.2 and are defined and characterised below. The (sub)biozones were determined by visualy appraising the relative abundance curves in Fig. 4.1, although some consideration was also given to the constrained cluster analysis (Fig. 4.3) which is based on the presence/absence of dinocyst and acritarch taxa.

The percentage abundance of each dinoflagellate cyst taxon is expressed relative to the total number of dinoflagellate cysts recorded for each sample. That of each marine acritarch taxon is based on the total number of marine acritarchs plus dinoflagellate cysts recorded for each sample, and that of *Tasmanites* sp. is also expressed relative to the total number of dinoflagellate cysts recorded for each sample.

The raw counts of woody debris (fragments >10 μm) and spores and pollen (Fig. 4.1) represent terrestrial influx. The assemblage biozones are based on a visual interpretation of the percentage abundances of the more common dinocyst and marine acritarch taxa and on the concentrations of dinocysts (Fig. 4.1) whereas the constrained cluster analysis (Fig. 4.3) is based on the presence or absence of dinocysts and acritarchs. The clusters revealed in Fig. 4.3 align remarkably closely with the assemblage biozones interpreted visually from the percentage abundances of common taxa (Fig. 4.1).

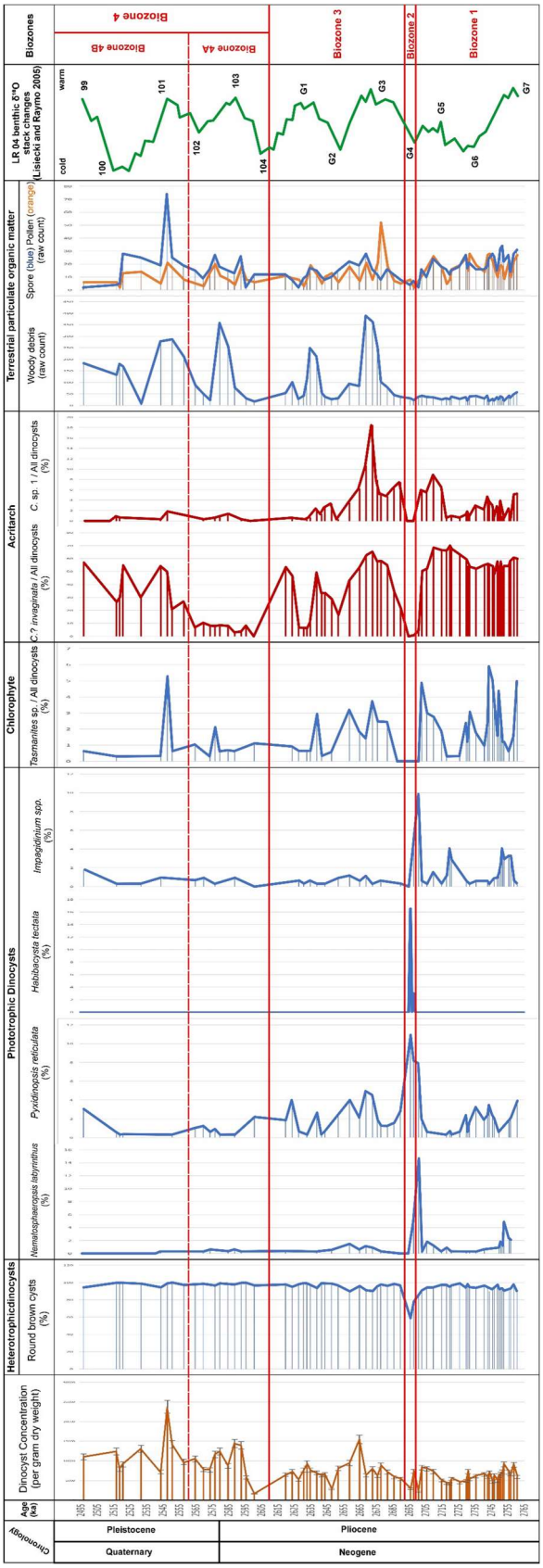
Biozones
Biozone 4
Biozone 4B
Biozone 4A
Biozone 3
Biozone 2
Biozone 1
LR 04 benthic δ18O stack changes (Lisiecki and Raymo 2005)
warm
cold
99
100
101
102
103
104
G1
G2
G3
G4
G5
G6
G7
Terrestrial particulate organic matter
Spore (blue) Pollen (orange) (raw count)
Woody debris (raw count)
Acritarch
C. sp. 1 / All dinocysts (%)
C.? invaginata / All dinocysts (%)
Chlorophyte
Tasmanites sp. / All dinocysts (%)
Phototrophic Dinocysts
Impagidinium spp. (%)
Habibacysta tectata (%)
Pyxidinopsis reticulata (%)
Nematosphaeropsis labyrinthus (%)
Heterotrophic dinocysts
Round brown cysts (%)
Dinocyst Concentration (per gram dry weight)
Age (Ma)
2495
2505
2515
2525
2535
2545
2555
2565
2575
2585
2595
2605
2615
2625
2635
2645
2655
2665
2675
2685
2695
2705
2715
2725
2735
2745
2755
2765
Chronology
Pleistocene
Pliocene
Quaternary
Neogene

Fig. 4.1. The more abundant dinocyst and acritarch taxa and informal biozones for the study interval in ODP Hole 882A. See text for the calculation of percentages and Fig. 4.2 for abundances of individual *Impagidinium* species. Samples 11-5, 132–134 cm (2694 ka, 101.64 m), 11-3, 62–64 cm (2612 ka, 97.94 m), 11-3, 42–44 cm (2605 ka, 97.74 m), and 11-1, 61–63 cm (2506 ka, 94.95 m) were excluded from this diagram as they contained only amorphous organic material. The benthic foraminiferal $\delta^{18}O$ stack of Lisiecki and Raymo (2005) is shown for comparison.

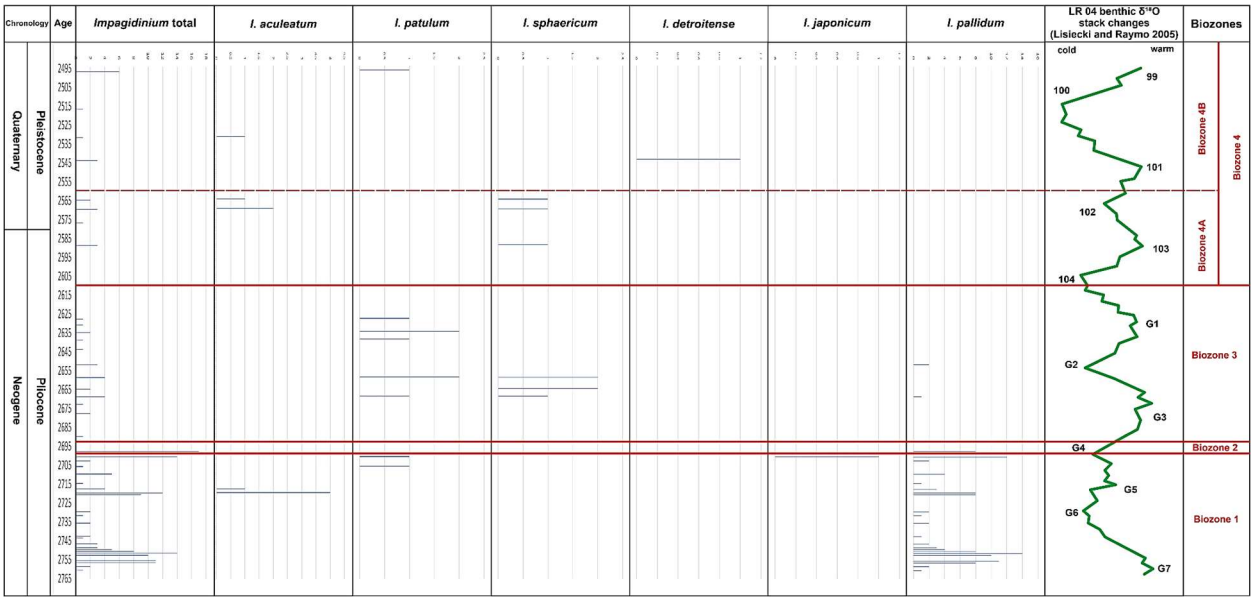

Fig. 4.2. Raw counts of *Impagidinium* species and informal biozones for the study interval in ODP Hole 882A. *Impagidinium* spp. total includes indeterminate species. Samples 11-5, 132–134 cm (2694 ka, 101.64 m), 11-3, 62–64 cm (2612 ka, 97.94 m), 11-3, 42–44 cm (2605 ka, 97.74 m), and 11-1, 61–63 cm (2506 ka, 94.95 m) were excluded from this diagram as they contained only amorphous organic material. The benthic foraminiferal $\delta^{18}O$ stack of Lisiecki and Raymo (2005) is shown for comparison.

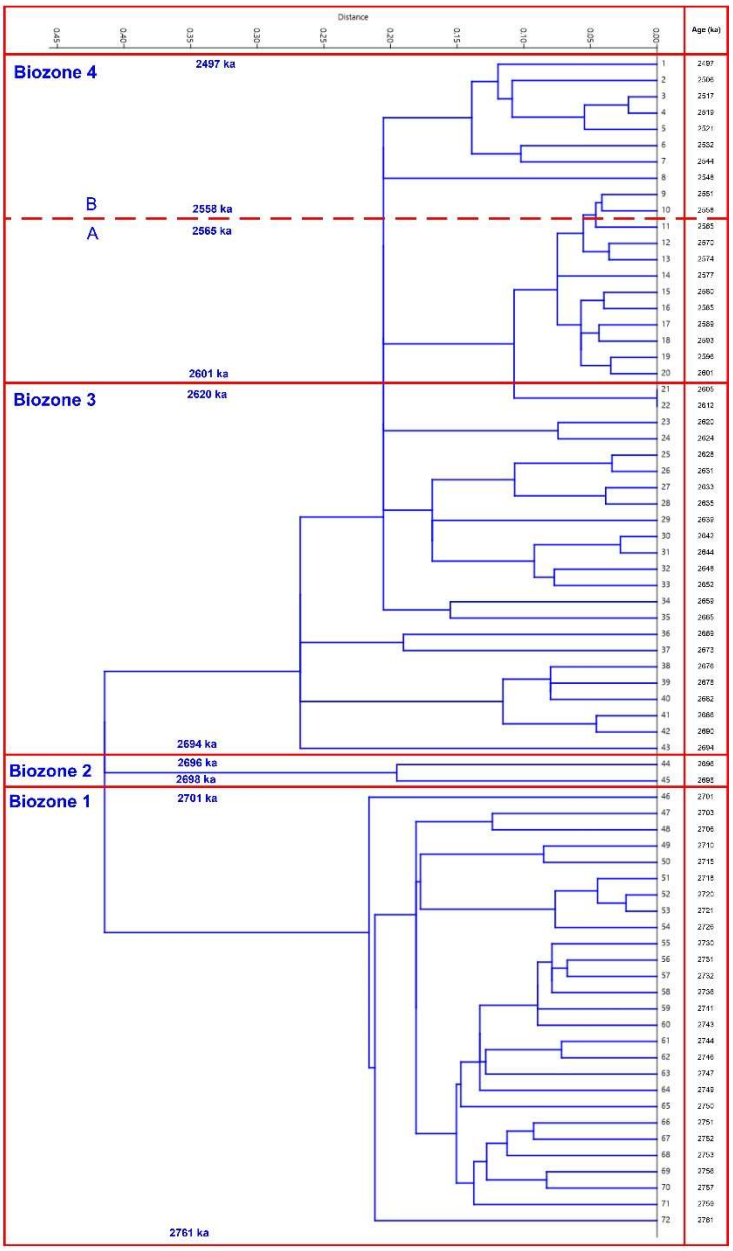

Fig. 4.3. Constrained cluster analysis dendrogram based on the presence/absence of dinocyst and acritarch taxa with biozone/ sub-biozone boundaries determined from Fig. 4.1. Samples are constrained stratigraphically from oldest (Sample 12-2, 66–68 cm; lab sample number 72) to youngest (Sample 11-1, 45–47 cm; lab sample number 1). This chart was generated using PAST software 4.04 (Hammer et al., 2021).

4.1.1. Marine Palynomorph Assemblage Biozone 1: Samples 12-2, 66–68 cm to 11-6, 22–24 cm, depth 105.98–102.04 m, age 2761–2701 ka

This biozone encompasses the lowermost part of this study. Round brown cysts dominate the dinocyst assemblages throughout this biozone. Their abundance ranges between 85% in the uppermost sample of this biozone (2701 ka) and 99% at a depth of 103.38 m (2726 ka). The declining numbers of round brown cysts mark the boundary between this biozone and Biozone 2, where they reach their lowest abundance throughout the entire interval of this study.

Overall, dinocyst concentrations are moderately high and range between 4095 (2720 ka) and 9071 (2753 ka) cysts per gram dry weight, with not much fluctuation recorded within this biozone.

Among the phototrophic dinocysts, *Impagidinium pallidum* is the most abundant species with relatively high numbers in the lowest samples reaching a maximum of 4% at 2752 ka, and declining upwards, and ranging between 1% at 2718 ka and 3% at 2721 and 2720 ka. They sharply increase in the uppermost sample to 8.5% at 2701 ka. The other species of the genus *Impagidinium* recorded in this biozone is *I. aculeatum*, appearing in two samples at 2720 ka (four specimens), and 2718 ka (one specimen).

Nematosphaeropsis labyrinthus and *P. reticulata* are present in small numbers, with *N. labyrinthus* showing a sharp peak of 14% in the highest sample of this biozone (2701 ka) and representing its highest abundance for the entire study.

The acritarch *C.*? *invaginata* is abundant and reaches 69% at 2720 ka. *Cymatiosphaera* sp. 1 is present and reaches 6% at 2703 ka. Both species show a pronounced peak at 2715 ka, with *C.*? *invaginata* registering 66% and *Cymatiosphaera* sp. 1 close to 6%. Both species decline towards the top of the biozone.

Tasmanites sp. is present in small numbers within this biozone, fluctuating throughout and ranging between 0 and 6%, with its highest abundance close to 6% at 2744 ka. Terrestrial spores and pollen are relatively abundant and woody debris is relatively low in abundance through this biozone.

4.1.2. Marine Palynomorph Assemblage Biozone 2: Samples 11-6, 4–6 cm and 11-5, 146–148 cm; depth 101.86 m to 101.78 m; age 2698 ka to 2696 ka.

This biozone encompasses only two samples and represents the total range of *Habibacysta tectata* (Fig. 4.4), this species comprising 3% (Sample 11-6, 4–6 cm) and 16% (Sample 11-5, 146–148 cm) of all dinocysts. *Pyxidinopsis reticulata* is relatively abundant, comprising 8% (lower sample) and 11% (upper sample). The relative abundance of round brown cysts declines and reaches its lowest values throughout the entire studied interval, these being 78% in the lower sample and 59% in the upper sample. *Impagidinium pallidum* peaks in this biozone, reaching 2% (8 specimens) in the lower sample and none in the upper sample. *Impagidinium patulum* and *I. japonicum* were each represented by one specimen in this biozone.

The acritarchs *C.*? *invaginata* and *Cymatiosphaera* sp. 1 are absent from these two samples, as is *Tasmanites* sp.

Dinocyst concentrations are relatively low compared with Biozones 1 and 3, with registered values between 7334 and 2801 cysts per gram dry weight. Terrestrial spores and pollen and woody debris are low in abundance through this biozone.

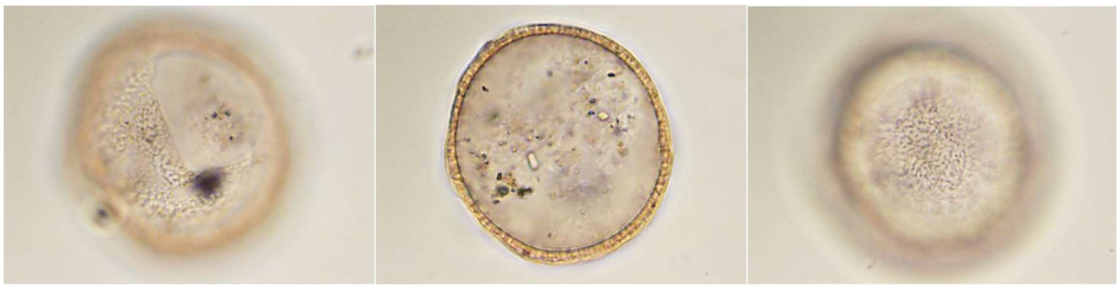

Fig. 4.4. *Habibacysta tectata* Head, 1994 in dorsal view, from left to right, dorsal surface, mid-focus, and ventral surface. Central body maximum diameter 58 µm. Sample 11–5, 146–148 cm; slide 1; England Finder reference E42/4. Age 2696 ka.

4.1.3. Marine Palynomorph Assemblage Biozone 3: Samples 11-5, 132–134 cm to 11-3, 86–88 cm; depth 101.64 m to 98.18 m; age 2694 ka to 2620 ka.

The upper boundary of this biozone (with Biozone 4) is represented by a gap in the data where two adjacent samples (11-3, 62–64 cm and 11-3, 42–44 cm) yielded a substantial amount of AOM and an unknown precipitate, these obscuring or diluting any palynomorphs that might be present. This gap is shown in Figs. 4.1–4.3.

The relative abundances of round brown cysts recover well in this biozone, with values between 93% at 2639 ka and 99% at 2633 ka.

Phototrophic dinocysts show reduced numbers in this biozone compared to Biozone 2. *Nematosphaeropsis labyrinthus* reaches a maximum of 1.5% in Sample 11-4, 122–24 cm at 2659 ka but is absent from many samples.

Pyxidinopsis reticulata also appears in small numbers during Biozone 3. This species is not present in a few samples but otherwise occurs in four peaks: 5% in Sample 11-5, 2–4 cm (2669 ka), 4% in Sample 11-4, 122–124 cm (2659 ka), 3% in Sample 11-4, 33–35 cm (2639 ka), and 4% in Sample 11-3, 103–105 cm (2624 ka).

Impagidinium pallidum is only present as two specimens in Sample 11-4, 104–106 cm (2652 ka) and *I. patulum* is present as just two specimens in Sample 11-4, 122–124 cm (2659 ka). The genus *Impagidinium* does not reach abundances greater than 1% (2659 ka) during this biozone.

The acritarchs *C.*? *invaginata* and *Cymatiosphaera* sp. 1 appear in great numbers during this biozone as with Biozone 1, with *C.*? *invaginata* varying from 6% in Sample 11-4, 0–2 cm at 2633 ka to 58% in Sample 11-5, 47–49 cm at 2678 ka. *Cymatiosphaera* sp. 1 has a highest abundance of 18% in Sample 11-5, 22–24 cm at 2673 ka and is absent from samples near the upper boundary of this biozone.

The terrestrial particulate organic matter (POM) shows two significant peaks in Biozone 3. Woody debris is most abundant in Samples 11-5, 2–4 cm at 2669 ka (389 pieces) and 11-4, 7–9 cm at

2635 ka (249 pieces). Sample 11-5, 2–4 cm at 2669 ka has the highest abundance of spores in this biozone (26 individual).

4.1.4. Marine Palynomorph Assemblage Biozone 4: Samples 11-3, 17–19 cm to 11-1, 45–47 cm; depth 97.49 m to 94.77 m; age 2600 ka to 2497 ka.

Round brown cysts predominate (94–100%) in all samples. *Impagidinium aculeatum* and *I. detroitense* are also present. There is abundant woody debris accompanied by small numbers of *Tasmanites* sp. and *Nematosphaeropsis labyrinthus*. Both species are quite rare. It is worth mentioning that *Tasmanites* sp. is most abundant in Samples 11-2, 4–6 cm (5% at 2548 ka) and 11-2, 101–103 cm (2% at 2577 ka).

Woody debris is present in all samples but they become quite abundant during interglacials (e.g., MIS 99 and 101). It is especially abundant in samples, 11-1, 146–148 cm (95.78 m), 11-2, 21–23 cm (96.03 m), and 11-2, 116–118 cm (96.97 m).

Cymatiosphaera? invaginata is moderately abundant at 57% in the youngest sample (11-1, 45–47 cm; 2497 ka), while it becomes quite rare closer to the Plio-Pleistocene boundary (3% at 2580 ka). The sharp and sustained rise in *C.*? *invagina* marks the boundary between **Sub-biozone 4A** and **Sub-biozone 4B**.

4.1.4.1. Marine Palynomorph Assemblage Sub-biozone 4A: Samples 11-3, 17–19 cm to 11-2, 62–64 cm; depth 97.49 m to 96.44 m; age 2600 ka to 2565 ka.

Within Sub-biozone 4A (2601–2565 ka) *C.*? *invagina* is absent at 2601 ka and reaches its highest abundance at 10% in Sample 11-2, 74–76 cm (2565 ka). Heterotrophic dinocysts dominate with abundances of 97–99% within this subzone. However, the dinocyst concentration of 1630 cysts per dry gram weight in this subzone in Sample 11-3, 33–35 cm (2601 ka) is the lowest concentration recorded in the entire study.

4.1.4.2. Marine Palynomorph Assemblage Sub-biozone 4B: Samples 11-2, 44–46 cm to 11-1, 45–47 cm; depth 96.26 m to 94.77 m; age 2558 ka to 2497 ka.

The sharp increase in the abundance of *C.*? *invaginata* defines the lower boundary of Biozone 4B (2558–2497 ka). This species rises to 57% at the top of this subzone in Sample 11-1, 45–47 cm (2497 ka).

Dinocyst concentrations are between 7,220 (2544 ka) and 14,198 cysts per gram dry weight (2551 ka), this being the highest concentration recorded within the present study.

Impagidinium detroitense is represented by a single specimen in this sub-biozone, in Sample 11-1, 146–148 cm, at 2544 ka (Appendix A).

4.2. Detrended Correspondence Analysis

DCA for the ODP Site 882 data set for all particulate matter (this study) is shown in Fig. 4.5. The ordination of samples shows no clear pattern, although the plot for taxa shows meaningful ordination.

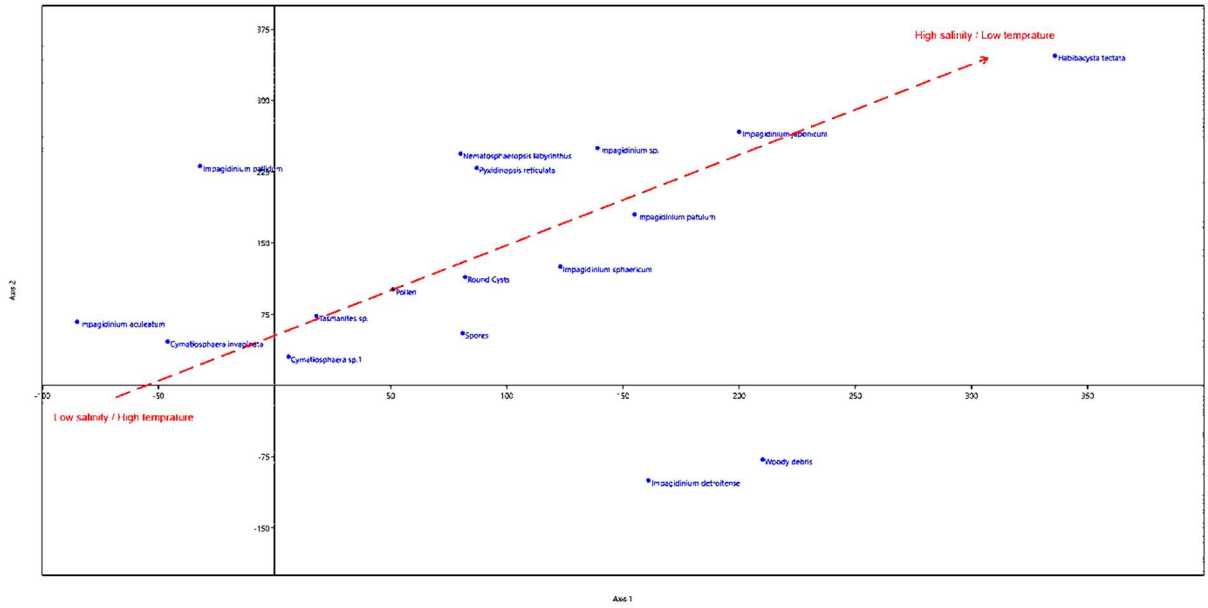

Fig. 4.5. Detrended correspondence analysis for all particulate organic matter counted from ODP Site 882 (this study). Axes 1 and 2 appear to represent predominantly components of temperature and salinity although it is unclear which axis is temperature and which is salinity.

Axis 1 and Axis 2 represent conditions with the most influential impact on the abundance of species (Dale and Dale, 2002). The lowest scores were calculated for the acritarchs *Cymatiosphaera*? *invaginata* and *Cymatiosphaera* sp. 1, and the dinocyst *Impagidinium aculeatum*. The alga *Tasmanites* sp. also shows a low score, and is plotted close to spores and

pollen, wheras round brown cysts show an intermediate score compared to all plotted particulate organic matter. The highest score was calculated for *Habibacysta tectata*.

Chapter 5: Discussion

In order to use cyst concentrations as a measure of biological productivity for cyst-forming dinoflagellates, it is necessary to remove the effects of changing sedimentation rates, especially as these vary between 11 and 2 cm/kyr across the interval of study (fig. 2 of Tiedemann and Haug, 1995; Fig. 5.1C). Cyst fluxes could not be determined because samples had not been collected by volume, so removal of the sedimentation rate effect was accomplished by normalizing each concentration value to a standardized rate of 5 cm/kyr (chosen somewhat arbitrarily to reflect the midpoint between the maximum and minimum rates over the studied interval). These adjusted cyst concentrations are plotted on Fig. 5.1B and reveal trends more reflective of productivity than those shown by raw cyst concentration values (Fig. 5.1A).

5.1. Biozone 1 (2761–2701 ka) and formation of the halocline

The lowest part of this biozone coincides with MIS G7 and it terminates at the MIS G5–G4 transition. Previous research on the geochemistry and hydrology of the North Pacific Ocean has indicated that the permanent halocline was formed around this time at ~2.73 Ma which coincides with the middle of Biozone 1 (e.g., Haug et al., 1995; Haug et al., 2005; Studer et al., 2012). The halocline today separates the upper 300-meter water from the water column below and reduces heat and nutrient exchange with the ocean's interior (Garett et al., 1991). This stratification increases the seasonal contrast of sea surface temperature (SST), which will have affected sea-surface productivity on a large scale (Levitus and Boyer, 1994; Haug et al., 2005). During the latest

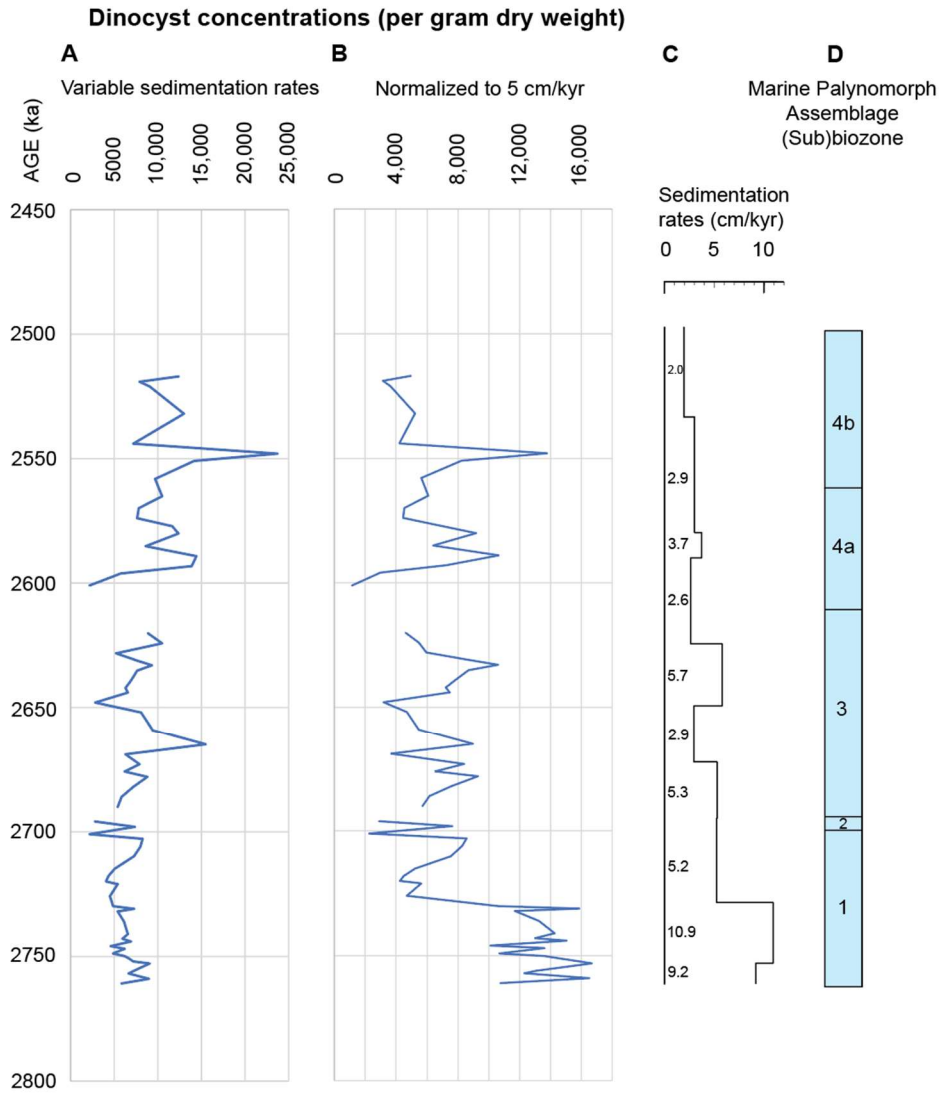

Fig. 5.1. Dinocyst concentrations for ODP Site 882 plotted against age. A) raw cyst concentration values; B) cyst concentration values normalized to a standardized rate of 5 cm/kyr to eliminate the effects of changing sedimentation rates over time; C) sedimentation rates for the interval of study based on the age model used herein (from fig. 2 of Tiedemann and Haug, 1995); D) Marine Palynomorph Zones and Subzones proposed in the present study.

Pliocene, the inability of surface water to exchange heat with deeper water caused the summer warm surface water to remain relatively warm through the fall, providing the moisture needed to expand major glaciation over North America at around 2.7 Ma (Haug et al., 2005), thereby intensifying Northern Hemisphere glaciation (Fig. 5.2).

Haug et al. (2005) reported a decrease in biogenic opal mass accumulation rates at ~2.73 Ma with the onset of the modern halocline at Site 882. This decrease paralleled a reduction in the levels of nutrients (Haug et al., 1999). A decrease in dinocyst species richness, along with a drop in sedimentation rates, was reported by Zorzi (2019) based on a low-stratigraphic-resolution study of the dinocysts from ODP Site 882 at 2.7 Ma. The present study shows that dinocyst taxonomic richness remained low (1 to 11 taxa) throughout the interval of this research. Zorzi (2019) also reported low species richness within the interval of the present study.

Throughout Biozone 1, and also through Biozones 3 and 4, elevated productivity is indicated by the overwhelming dominance of round brown cysts. In Biozone 1, the changes in the concentrations of dinocysts match changes in MISs fairly well. Their values are greatest at interglacial MIS G7 with maximum concentrations at 2753 ka, indicating highly productive sea-surface conditions. At around 2720 ka, there is a noticeable decrease in productivity as inferred from the dinocyst concentrations that coincides with the intensification of Northern Hemisphere glaciation at MIS G6.

After a rise in concentrations, coinciding with interglacial MIS G5, a decline to minimum concentrations occurs at 2701 ka coincident with the onset of glacial MIS G4. Nonetheless, the fluctuation in dinocyst concentrations does not vary widely across this biozone, suggesting *prima*

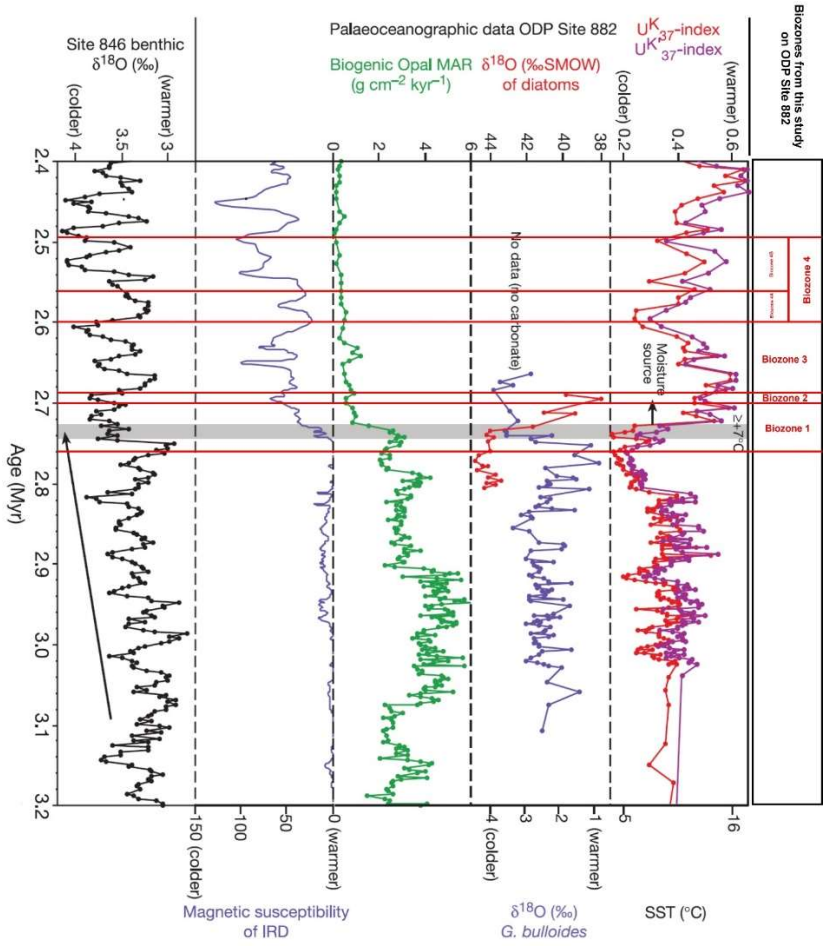

Fig. 5.2. Paleoceanographic data for ODP Site 882 modified after Haug et al. (2005) with biozones from this study. The arrow points to the intensification of Northern Hemisphere glaciation and the grey bar to the onset of halocline formation. Note that at this time there is a drop in magnetic susceptibility of ice-rafted debris (IRD) pointing to a colder late Pliocene and Pleistocene, while the alkenone unsaturation ratios (U^{K}_{37} index) reflect higher summer sea surface temperatures. In the western subarctic Pacific, coccolithophorids, which produce alkenones, generally bloom in the middle to late summer (From Haug et al., 2005).

face that dinocyst production was not greatly influenced by the formation of the halocline. However, sedimentation rates during Biozone 1 are 9.2–10.9 cm/kyr from the base upwards, and then drop to 5.2 cm/kyr at 2.73 Ma and thereafter (Tiedmann and Haug, 1995; Fig. 5.1C). This represents almost a halving in the rate of cysts reaching the ocean floor during the upper half of Biozone 1 (Fig. 5.1B), and hence a significant and rapid decrease in implied productivity. Dinocyst production therefore diminished sharply with the onset of stratification.

Across Biozone 1, the acritarch species show a signifcant trend in response to climate cycles. *Cymatiosphaera*? *invaginata* and *Cymatiosphaera* sp. 1 both become more abundant around the interglacial MIS G7 and G5, whereas their numbers decline during glacial MIS G6 and G4. Even though the global distribution of *Cymatiosphaera*? *invaginata* shows a strong correlation with polar and sub-polar waters, it appears to thrive with an increase in the influx of nutrients from terrestrial sources. This is consistent with the hypothesis that *Cymatiosphaera*? *invaginata* responded positively to reduced salinity as suggested by previous research from the northern North Pacific region (Zorzi et al., 2020; Haj Soltan, 2021).

Impagidinium pallidum is the best represented species of its genus in this biozone where it also has its highest abundance (4% at 2752 ka) in the entire study (Chapter 4, Appendix 2). This species is most abundant at the MIS G7–G6 transition around 2755–2745 ka, prior to the formation of the modern halocline, and is an indicator of cool surface waters (Zorzi, 2019; Zorzi et al., 2020; de Vernal et al., 2020).

5.2. Biozone 2 (2698–2696 ka) and a significant change in palynological assemblages

Biozone 2 marks a significant change in the palynological assemblages at 2698–2696 ka, which coincides with the glacial MIS G4. During this short interval, a drop in the abundance of terrestrial particulate organic matter was reported by Zorzi (2019), and very low values are confirmed in the present study. However, there is a significant accompanying change in the dinocyst assemblages. *Habibacysta tectata* is restricted to this short biozone and reaches 16% of the assemblages. This species was reported to be quite abundant before 4.2 Ma at Site 882 (Zorzi, 2019) and is a well-known cold-tolerant species (Head, 1994). *Pyxidinopsis reticulata* also has its highest abundance (11%) in this biozone. Based on its modern distribution in the Arctic, de Vernal et al. (1998) and Radi and de Vernal (2008) noted a slight positive correlation between its relative abundances and sea ice cover duration. This is in parallel with a wider range of changes recorded in the magnetic susceptibility of ice rafted debris from ODP Site 882 (Rea et al., 1993; Fig 5.2), which is not seen before 2.73 Ma.

Round brown cysts reach their minimum relative abundance (58%) throughout the entire interval of this study. Cyst concentrations are also low. At the same time, an abrupt decrease in diatom abundance is followed by the disappearance of pyritized diatom specimens (Appendix 2), which coincides with a drop in biogenic opal mass accumulation rates (Fig. 5.2), suggesting low sea-surface productivity at this time. These data suggest reduced nutrients or cool surface waters, or both, during glacial MIS G4. The near disappearance of acritarch species, as well as woody debris and pollen and spores, also confirms a pronounced environmental perturbation at this time.

The dinocyst record indicates that the sea surface was ice-free at least during the summer, permitting a light source for phototrophic dinocysts. However, modeling by Haug et al. (2005, Fig. 5.2) showed particularly low summer sea-surface temperatures at ~2.70 Ma.

5.3. Biozone 3 (2694–2620 ka) and larger amplitude of changes

Across Biozone 3, heterotrophic round brown cysts become dominant again. With the start of interglacial MIS G3, sea-surface conditions appear to recover rapidly from the intense glacial MIS G4. Pyritized diatom fragments become quite abundant again based on current observations, indicating the availability of food for heterotrophic dinoflagellates (Chapter 4; Appendix 2). There is a slow but noticeable increase in biogenic opal mass accumulation rates within this biozone after Biozone 2, reaching a maximum of 1.17 g/cm^{2}ky at 2642 ka (Haug and Sarnthein, 2005). However, the overall mass accumulation rates of biogenic opal never reach the high values of before 2.73 Ma, when the halocline was formed (Rea et al., 1993; Haug and Sarnthein, 2005; Haug et al., 2005; Fig. 5.2).

Phototrophic dinoflagellates, as well as *Tasmanites* sp., appear to thrive during interglacial MIS G3 and G1, showing two major peaks in abundance. Dinocyst concentrations increase after Biozone 2. However, sedimentation rates are between 2.6 and 5.7 cm/kyr during Biozone 2 and 3, as compared with 10.9 cm/kyr for the lower half of Biozone 1 (Tiedmann and Haug, 1995; Fig. 5.1C). These low sedimentation rates mean that productivity continues to be much lower than implied by the cyst concentrations (Fig. 5.1B). Even so, a wide range of dinocyst concentrations is recorded in Biozone 3, from 15467 dinocysts at around MIS G3 to only 2780 dinocysts at MIS

G2. This wide range in inferred productivity is not seen in Biozone 1 and seems to reflect the increasing amplitude of glacial–interglacial oscillations in the latest Pliocene.

The acritarch species, *C.*? *invaginata* and *Cymatiosphaera* sp. 1 become quite abundant around the time of MIS G3. Their peak matches the peak in terrestrial particulate organic matter, confirming that the terrestrial influx and presumably low-salinity water was quite high, and nutrients were available for microorganisms to thrive. These peaks in acritarch numbers also reinforce the links at least between *C.*? *invaginata* and reduced salinity, warmer sea-surface temperatures, and enhanced nutrients at high northern latitudes.

The abundance of woody debris is conspicuous in this biozone. These organic particles, together with pollen and spores appear in great numbers in interglacial periods in Biozones 3 and 4, possibly because of prolonged summers as suggested by previous research (Haug et al., 1999; Haug et al., 2005).

5.4. Biozone 4 (2600–2497 ka) and recovery from a low productive period

Sub-biozone 4A (2600–2565 ka) has fairly consistent and low sedimentation rates of 2.6–3.7 cm/kyr, as compared with up to 5.7 cm/kyr during Biozones 2 and 3 (Tiedemann and Haug, 1995; Fig. 5.1C). Dinocyst concentrations are at their lowest (1630 per gram dry weight) in the lowest sample at 2601 ka, which coincides with glacial MIS 104. Otherwise, allowing for the low sedimentation rates, concentrations suggest approximately similar productivity to Biozone 3 (Fig. 5.1B), and round brown cysts continue to predominate throughout. Somewhat higher cyst concentrations are recorded in interglacial MIS 103 and a decline coincides with glacial MIS 102.

Terrestrial influx is variable through Sub-biozone 4A, and a pronounced peak in woody debris corresponds with interglacial MIS 103. Palynological data suggest that during Biozone 4A, conditions were relatively productive despite the presence of an established halocline (Haug et al., 1999), given that round brown cysts dominate all assemblages in this biozone.

However, conspicuously, low abundances of the acritarchs *C.*? *invaginata* and *Cymatiosphaera* sp. 1 characterise Sub-biozone 4A. Their low abundance, particularly in MIS 103 where this might not be expected, might signify elevated salinities throughout Sub-biozone 4A. Also, the magnetic susceptibility of IRD shows a peak implying colder conditions during this sub-biozone even though it coincides with the warm period of MIS 103, supporting lower precipitation and higher salinity (Rea et al., 1993; Fig. 5.1).

Sub-biozone 4B (2558–2497 ka) is characterized by a return to abundant *Cymatiosphaera*? *invaginata* which maintains high values in both glacial MIS 100 and interglacial MISs 101 and 99, implying a return to lower salinities and perhaps enhanced nutrient levels. Increases in terrestrial particulate organic matter support this interpretation. Dinocyst concentrations remain at comparable levels to those in Sub-biozone 4A, sedimentation rates remain relatively low at 2.9–2.0 cm/kyr (Tiedemann and Haug, 1995; Fig. 5.1C), and round brown cysts continue to predominate throughout. This all suggests somewhat reduced but comparable productivity to Sub-biozone 4A (Fig. 5.1B).

During the interglacial MIS 101 and 99 within this sub-biozone, large fragments of woody debris and other plant tissues become very abundant, unlike any other interval in this study. Moreover,

there is a noticeable increase in the abundance of pollen and spores as well as the remains of invertebrates (copepods?) during MIS 101 and 99 (Chapter 4, Appendix 2). Such an association suggests that during these marine isotope stages, this part of the Subarctic Gyre was under the heavy influence of river discharge. This will have led to nutrient input and enhanced productivity and reduced salinity, which seems to explain the high abundances of *Cymatiosphaera*? *invaginata*.

Impagidinium detroitense is restricted to Sub-biozone 4B in the present study where it is represented by a single specimen in Sample 11-1, 146–148 cm, dated at 2544 ka (Appendix 1). This observation extends the range of this species to 2544 ka, having formerly been recorded between 5270 and 2700 ka in the northern North Pacific (Zorzi et al., 2019).

General comments. Throughout Biozone 4, invertebrate remains are more abundant during the warmer climate cycles (Appendix 2). These remains are mainly possible eggs of invertebrate organisms (>50 um) and their whole-body exoskeletons (>100 um). These organisms feed on smaller planktonic organisms such as diatoms and dinoflagellates. Abundances of the acritarch *C.*? *invaginata* decline as invertebrate remains, including their interpreted eggs, increase in samples through this biozone (Appendix 2).

Overall, dinocyst concentrations remain at fairly significant levels (mostly between 7,000 and 15,000 cysts per gram dry weight; Fig. 5.1A) throughout Biozone 4, except for the lowest few samples, and round brown cysts remain the dominant dinocyst group throughout, implying moderately high surface water productivity during both glacial and interglacial climate cycles. *Impagidinium* spp. and *Pyxidinopsis reticulata*, although rare, become somewhat more abundant

during these cold stages. The character of these assemblages indicates that the surface waters were ice-free during summer, and these findings are consistent with the hypothesis of Haug et al. (1999; 2005) and Swann et al. (2006) that warm surface waters extended into late summer and fall.

5.5. Autecology inferred from Detrended correspondence analysis

The results of DCA are shown in Fig. 4.5. The acritarch *Cymatiosphaera*? *invaginata* has been reported in abundance from the Upper Pliocene–Lower Pleistocene transition of the Bering Sea and is generally associated with high latitudes and reduced salinity conditions (HajSoltan, 2021 and references therein). Since the abundance of *Cymatiosphaera* sp. 1 changes in parallel with *C.*? *invaginata*, it may be concluded that these species thrive in similar conditions. Both species peak in interglacial periods throughout this study (Chapter 4). The dinocyst *Impagidinium aculeatum* is most abundant today in low- to mid-latitude oceanic and oligotrophic environments (Zonneveld et al., 2010; 2013; de Vernal et al., 2020) and is found only in low numbers in the northern North Pacific where salinities and temperatures are relatively low (Bonnet et al., 2012; de Vernal et al., 2020).

The alga *Tasmanites* sp. plots near spores and pollen, which represent increased freshwater influence, and peaks in warm periods throughout this study. *Tasmanites* sp. does not however show a trend closely similar to that of the acritarchs (Chapter 4).

Round brown cysts show an intermediate score compared to all plotted particulate organic matter. They are reported from a wide range of settings (Zonneveld et al., 2013). As

heterotrophs, their distributions are largely influenced by those of their prey, which includes diatoms, and so are often associated with elevated nutrients (Dale, 1996). They include species of the genus *Brigantedinium*, a euryhaline opportunistic genus that is abundant in the northern North Pacific and Bering Sea today (Bonnet et al., 2012).

Habibacysta tectata has the highest score and appears only in the glacial MIS G4. It is a known cool-tolerant species (Head, 1994).

Impagidinium detroitense and *Impagidinium pallidum* do not fall within the observed trend. *Impagidinium detroitense* is represented by a single specimen which might account for its unusual score. This Pliocene–Pleistocene species was discovered only recently from the northen North Pacific (Zorzi et al., 2019) and its paleoecology is not well understood. The genus *I. pallidum*, on the other hand, is quite abundant within Biozone 1 (Chapter 4) and its score could be an indication that this species is dependent on parameters other than temperature and salinity. This polar species is highly dependent on phosphate and nitrate (Zonneveld et al., 2013). After the formation of halocline, the abundance of this species declines along with the decrease in the concentrations of nitrogen (Swann et al., 2006; Studer 2013; Haug et al., 2005). Thus, it appears that the score of *Impagidinium pallidum* is related to temperature and levels of nutrients, rather than temperature and salinity (Fig. 4.5).

Chapter 6. Summary and Conclusions

ODP Site 882 is located on the Detroit Seamount of the Emperor Seamount Chain in the western Subarctic Gyre of the northern North Pacific. It is significant because the analyses of sediments recovered from here were used to propose that modern stratification of the water column was initiated at ~2.73 Ma, and that this caused the intensification of Northern Hemisphere glaciation during the latest Pliocene (Haug et al., 2005). The present palynological study is based on 72 samples spanning the Pliocene–Pleistocene transition across the interval 2497 ka to 2761 ka. A total of 68 samples were found to contain dinocysts, with preservation being good to moderate, but characterized by low taxonomic richness (a total of 11 taxa). Assemblages reveal an overwhelming dominance of heterotrophic round brown cysts in almost all samples. These pale yellow to dark brown cysts, as well as abundant pyritized diatoms, indicate productive sea surface conditions despite the decrease in nutrient levels caused by the formation of a persistent halocline since ~2.73 Ma (Haug et al., 2005). Previous reports from two sites in the North Pacific Ocean (Zorzi, 2019) and Bering Sea (HajSoltan, 2021) indicate low-salinity surface waters at this time, opening the possibility of an increased rate of precipitation or influx of fresher water (e.g., Haug et al., 1995; 1999; 2005; Zorzi, 2019; Zorzi et al., 2020).

The formation of a halocline at ~2.73 Ma within Biozone 1 (2761–2701 ka) is reflected in an overall reduction in productivity, marked by an abrupt drop in biogenic opal mass accumulation rates (Haug et al., 1995). However, dinocyst assemblage composition does not show significant or abrupt changes at this time, and cyst concentrations are relatively constant through Biozone 1 except for the highest sample. The main change is the reduced sedimentation rate, from 10.9

cm/kyr from near the base of Biozone 1 upwards, and then a significant drop to 5.2 cm/kyr at 2.7 Ma and further declines thereafter (Tiedmann and Haug, 1995; Fig. 5.1C), implying a ~50% drop in dinocyst recruitment to the ocean floor at 2.73 Ma (Fig. 5.1B). This aside, the onset of stratification does not seem to have had a pronounced effect on the dinocyst record. However, assemblages older than 2750 ka show relatively higher taxonomic richness including specimens of the genus *Impagidinium*, indicating higher salinities, and especially *I. pallidum* which also indicates lower sea-surface temperatures (de Vernal et al., 2020).

There is a significant change in dinocyst assemblages between 2698–2696 ka defining Biozone 2 which is coincident with glacial MIS G4. A drop in the abundance of terrestrial particulate organic matter and of heterotrophic round brown cysts and an increase in the abundance of *Pyxidinopsis reticulata* are suggestive of reduced productivity and cooler surface waters, an interpretation supported by the peak abundance of *Habibacysta tectata* which is a cold-tolerant species (Head, 1994). Nonetheless, phototrophic dinocysts occurring in relatively high numbers within this biozone indicate ice-free conditions for at least the summer months.

Round brown cysts predominate again with the onset of Biozone 3 (2694–2620 ka) coincident with a slight increase in biogenic opal mass accumulation rates (Haug and Sarnthein, 2005). Dinocyst concentrations show greater fluctuations within this biozone than in Biozone 1 and reflect an increase in the amplitude of climate cycles during the latest Pliocene. Moreover, wide variations in the abundance of *Cymatiosphaera*? *invaginata* within this biozone suggest intervals of low surface salinity in the northern North Pacific during cold as well as warm stages.

The interval from 2600 to 2497 ka represents Biozone 4, which is divided into sub-biozones 4A and 4B primarily from the abundance of the acritarch *Cymatiosphaera*? *invaginata*. Sub-biozone 4A (2600–2565 ka) spans the Pliocene–Pleistocene boundary at 2.58 Ma. In the lowest part of this subzone, dinocyst concentrations are at their lowest in the entire study in spite of low sedimentation rates, and suggest low productivity coinciding with glacial MIS 104 at 2.6 Ma. This may be significant because MIS 104 is associated with a major glacial advance in the northern North Atlantic, with evidence of severe cooling across the higher latitudes of the Northern Hemisphere (Bailey et al., 2013; Hennissen et al., 2014, 2015). Otherwise, round brown cysts dominate all assemblages in this biozone, suggesting relatively high productivity. The low abundances of *Cymatiosphaera*? *invaginata* throughout this biozone, including interglacial MIS 103, suggest reduced precipitation and hence higher salinities at this time. Sub-biozone 4B (2558–2497 ka) registers a return to sporadically abundant *Cymatiosphaera*? *invaginata* in glacial MIS 100 and interglacial MISs 101 and 99, suggesting the return of reduced salinities and perhaps enhanced nutrient levels. In general, productivity seems to remain relatively unchanged although with a peak in interglacial MIS 101.

The dinocyst record throughout the studied interval, characterized by an overall dominance of round brown cysts, scarcity of phototrophs including *Impagidinium* species, and low taxonomic richness generally, reflects the harsh conditions and reduced salinities but elevated nutrient levels of the North Pacific Subarctic Gyre. Modest fluctuations in assemblage compositions, but significant shifts in both cyst concentrations and abundances of the acritarch *Cymatiosphaera*? *invaginata*, nonetheless reveal detailed variations at the level of individual climate cycles including significant changes following the establishment of the modern halocline at ~2.73 Ma.

Productivity evidently remained fairly high even during glacial cycles, including the intense glacial MIS G4, implying ice-free conditions at least during the summer. Surface salinities in general seem to have been somewhat higher during glacial intervals, which would be consistent with increased precipitation and river input during interglacials.

Most species recorded occur within their published stratigraphic ranges. However, this study extends the highest occurrence of *Impagidinium detroitense* Zorzi et al., 2020 from the Upper Pliocene at 2700 ka (Zorzi, 2019; Zorzi et al., 2020) to the Lower Pleistocene at 2544 ka.

References

Ao, H., Dekkers, M.J., Qin, L., Xiao, G., 2011. An updated astronomical timescale for the Plio-Pleistocene deposits from South China Sea and new insights into Asian monsoon evolution. Quat. Sci. Rev. 30, 1560–1575.

Balota, E.J., Head, M.J., Okada, M., Suganuma, Y., Haneda, Y., 2021. Paleoceanography and dinoflagellate cyst stratigraphy across the Lower–Middle Pleistocene Subseries (Calabrian–Chibanian Stage) boundary at the Chiba composite section, Japan. Prog. Earth Planet. Sci., 8(1), 1–38.

Budyko, M.I., Ronov, A.B., Yanshin, A.I., 1987. The history of the Earth atmosphere. English translation. Springer: Berlin; Gidrometeoizdat 1– 139.

Bogus, K., Mertens, K. N., Lauwaert, J., Harding, I. C., Vrielinck, H., Zonneveld, K. A., Versteegh, G. J., 2014. Differences in the chemical composition of organic-walled dinoflagellate resting cysts from phototrophic and heterotrophic dinoflagellates. J. Phycol., 50(2), 254–266.

Bonnet, S., de Vernal, A., Gersonde, R., Lembke-Jene, L., 2012. Modern distribution of dinocysts from the North Pacific Ocean (37–64°N, 144°E–148°W) in relation to hydrographic conditions, sea-ice and productivity. Mar. Micropaleontol., 84–85: 87–113.

Boyer, T.P., J.I. Antonov, O.K. Baranova, C. Coleman, H.E. Garcia, A. Grodsky, D.R. Johnson, R.A. Locarnini, A.V. Mishonov, T.D. O'Brien, C.R. Paver, J.R. Reagan, D. Seidov, I.V. Smolyar, M.M.

Zweng, 2013. World Ocean Database 2013. Sydney Levitus, S. (Ed.), NOAA Atlas NESDIS 72, 209 pp.

Chisholm, S.W., Morel, F.M.M. (Eds.), 1991. What controls phytoplankton production in nutrient-rich areas in the open sea? Limnol. Oceanogr. 36, 1507–1970.

Dale, A., Dale, B., 2002. Applications of ecologically based statistical treatments to micropaleontology. In: Haslett, S.K., Quaternary environmental micropalaeontology. Arnold: London, p. 260–286.

de Vernal, A., Henry, M., Matthiessen, J., Mudie, P.J., Rochon, A., Boessenkool, K.P., Eynaud, F., Grøsfjeld, K., Guiot, J., Hamel, D., Harland, R., Head, M.J., Kunz-Pirrung, M., Levac, E., Loucheur, V., Peyron, O., Pospelova, V., Radi, T., Turon, J.-L., and Voronina, E. 2001. Dinoflagellate cyst assemblages as tracers of sea-surface conditions in the northern North Atlantic, Arctic and sub-Arctic seas: the new 'n = 677' data base and its application for quantitative palaeoceanographic reconstruction. J. Quat. Sci., 16(7), 681–698.

de Vernal, A., Gersonde, R., Goosse, H., Seidenkrantz, M.S., Wolff, E.W., 2013. Sea ice in the paleoclimate system: the challenge of reconstructing sea ice from proxies – an introduction. Quat. Sci. Rev., 79, 1–8.

de Vernal, A., Radi, T., Zaragosi, S., Van Nieuwenhove, N., Rochon, A., Allan, E., De Schepper, S., Eynaud, F., Head, M.J., Limoges, A., Londeix, L., Marret, F., Matthiessen, J., Penaud, A., Pospelova, V., Price, A., Richerol, T., 2020. Distribution of common modern dinoflagellate cyst

taxa in surface sediments of the Northern Hemisphere in relation to environmental parameters: The new n=1968 database. Mar. Micropaleontol. 159, 101796, p. 1–23.

De Schepper, S., Head, M.J., 2014. New late Cenozoic acritarchs: evolution, palaeoecology and correlation potential in high latitude oceans. J. System. Palaeontol., 12(4), 493–519.

Galbraith, E.D., Samuel, L.J., Thomas, F.P., Daniel, M.S., Gerald, H.H., Mea, C., John, R.S., Roger, F., 2007. Carbon dioxide release from the North Pacific abyss during the last deglaciation. Nature, 449(7164), 890. doi: 10.1038/nature06227.

Gargett, A.E., 1991. Physical processes and the maintenance of nutrient-rich euphotic zones. Limnol. Oceanogr. 36, 1527–1546.

Hackett, J.D., Anderson, D.M., Erdner, D.L., Bhattacharya, D., 2004. Dinoflagellates: a remarkable evolutionary experiment. Am. J. Bot., 91(10), 1523–1534.

HajSoltan, F., 2021. Paleoceanography across the Pliocene–Pleistocene transition in the southern Bering Sea: dinoflagellate cysts and acritarchs from IODP Site U1341. Unpublished MSc thesis, Brock University.

Hammer, Ø., Harper, D.A.T., Ryan, P.D., 2001. PAST: Paleontological statistics software package for education and data analysis. Palaeontologia Electronica 4(1): 9pp. http://palaeo-electronica.org/2001_1/past/issue1_01.htm

Harada, N., Sato, M., Shiraishi, A., Honda, M., 2006. Characteristics of alkenone distributions in suspended and sinking particles in the northwestern North Pacific. Geochim. Cosmochim. Acta, 70, 2045–2062.

Haug, G.H., Ganopolski, A., Sigman, D., Rosell-Mele, A. et al., 2005. North Pacific seasonality and the glaciation of North America 2.7 million years ago. Nature 433, 821–825.

Haug, G.H., Sigman, D., Tiedemann, R., Pedersen, T., Sarnthein, M., 1999. Onset of permanent stratification in the subarctic Pacific Ocean. Nature 401, 779–782.

Head, M.J., 1994. Morphology and paleoenvironmental significance of the Cenozoic dinoflagellate genera *Tectatodinium* and *Habibacysta*. Micropaleontol., 289–321.

Head, M.J., 1996. Modern dinoflagellate cysts and their biological affinities. In Jansonius, J. and McGregor, D.C. (Eds.), Palynology: principles and applications. American Association of Stratigraphic Palynologists Foundation, Dallas, Texas, vol. 3, p. 1197–1248.

Hennissen, J.A.I., Head, M.J., De Schepper, S., Groeneveld, J., 2014. Palynological evidence for a southward shift of the North Atlantic current at 2.6 Ma during the intensification of late Cenozoic Northern Hemisphere glaciation. Paleoceanogr. 29, 564–580.

Hennissen, J.A.I., Head, M.J., De Schepper, S., and Groeneveld, J., 2015. Increased seasonality during the intensification of Northern Hemisphere glaciation at the Pliocene–Pleistocene boundary ~2.6 Ma. Quat. Sci. Rev., 129: 321–332.

Janouskovec, J., Gavelis, G.S., Burki, F., Dinh, D., Bachvaroff, T.R., and 10 others, 2016. Major transitions in dinoflagellate evolution unveiled by phylotranscriptomics. PNAS, www.pnas.org/cgi/doi/10.1073/pnas.1614842114; E171–E180.

Keir, R., 1988. On the Late Pleistocene ocean geochemistry and circulation. Paleoceanogr. 3, 413–447.

Kurita, H., Obuse, A., 2003. Dinoflagellate cyst biostratigraphy of ODP Hole 186 – 1151A sediments. Supplement to Kurita, H., Obuse, A., 2003. Middle Miocene–Uppermost Lower Pliocene Dinoflagellate Cyst Biostratigraphy, ODP Leg 186 Hole 1151A of Sanriku Coast of northern Japan, northwestern Pacific. In: Suyehiro, K., Sacks, I.S., Acton, G.,D., Oda, M., (Eds.) Proc. ODP Sci. Results 186 Coll. Stn. TX Ocean Drill. Program 1–19.

Legrand, J., Yamada, T., Terada, K., Nishida, H., 2021. Palynofloras from the Itsuki and Kuwajima formations of the Tetori Group and their correlation with paleofloristic provinces of eastern Asia. Paleontol. Res., 25(3), 177–190.

Limoges, A., Van Nieuwenhove, N., Head, M.J., Mertens, K.N., Pospelova, V., Rochon, A., 2020. A review of rare and less well known extant marine organic-walled dinoflagellate cyst taxa of the orders Gonyaulacales and Suessiales from the Northern Hemisphere. Mar. Micropaleontol. 159: 101801, p. 1–20.

Lisiecki, L.E., Raymo, M.E., 2007. Plio-Pleistocene climate evolution: Trends and transitions in glacial cycle dynamics. Quat. Sci. Rev. 26, 56–69.

Matsuoka, K., Bujak, J.P., Shimazaki, T., 1987. Late Cenozoic dinoflagellate cyst biostratigraphy from the west coast of Northern Japan. Micropaleontol. 33, 214–229.

Mertens, K.N., Gu, H., Gurdebeke, P.R., Takano, Y., Clarke, D., Aydin, H., Li, Z., Pospelova, V., Shin, H.H., Li, Z., Matsuoka, K., Head, M.J., 2020. A review of rare, poorly known, and

morphologically problematic extant marine organic-walled dinoflagellate cyst taxa of the orders Gymnodiniales and Peridiniales from the Northern Hemisphere. Mar. Micropaleontol., 159: 101773, p. 1–35.

Miyoshi, N., Fujiki, T., Morita, Y., 1999. Palynology of a 250-m core from Lake Biwa: a 430,000-year record of glacial–interglacial vegetation change in Japan. Rev. Palaeobot. Palynol., 104(3–4), 267–283.

Mochizuki, M., Shiga, N., Saito, M., Imai, K., Nojiri, Y., 2002. Seasonal changes in nutrients, chlorophyll a and the phytoplankton assemblages of the western subarctic gyre in the Pacific Ocean, Deep Sea Res., Part II, 49, 5421–5439.

Onodera, J., Takahashi, K., 2005. Silicoflagellate fluxes and environmental variations in the northwestern North Pacific during December 1997–May 2000, Deep Sea Res., Part I, 52, 371– 388.

Rea, D.K., Basov, I.A., Janecek, T.R., Palmer-Julson, A., et al., 1993. Proc. ODP, Init. Repts., 145: College Station, TX (Ocean Drilling Program), 85–119.

Rochon, A., de Vernal, A., Turon, J. L., Matthießen, J., Head, M. J., 1999. Distribution of recent dinoflagellate cysts in surface sediments from the North Atlantic Ocean and adjacent seas in relation to sea-surface parameters. Am. Assoc. Stratigraphic Palynologists Contrib. Ser, 35, 1–146.

Reid, J.L., 1969. Sea surface temperature, salinity, and density of the Pacific Ocean in summer and in winter. Deep-Sea Res. 16 (suppl.), 215–224.

Schlitzer, R., 2018. Ocean Data View. https://odv.awi.de.

Sigman, D.M., Jaccard, S.L., Haug, G.H., 2004. Polar ocean stratification in a cold climate. Nature, 428(6978), 59–63.

Stockmarr, J.A., 1971. Tablets with spores used in absolute pollen analysis. Pollen Spores, 13, 615–621.

Swann, G.E.A., Maslin, M.A., Leng, M.J., Sloane, H.J., Haug, G.H., 2006. Diatom $\delta^{18}O$ evidence for the development of the modern halocline system in the subarctic northwest Pacific at the onset of major Northern Hemisphere glaciation. Paleoceanogr., 21, PA1009.

Swann, G.E.A., Kendrick, C.P., Dickson, A.J., Worne, S., 2018. Late Pliocene marine pCO^2 reconstructions from the subarctic Pacific Ocean. Paleoceanography and Paleoclimatology, 33, 457-469. https:// doi.org/10.1029/2017PA003296

Talley, L.D. , 1993. Distribution and formation of North Pacific intermediate water. J. Phys. Oceanogr. 23, 517–537.

Tian, J., Wang, P., Cheng, X., Li, Q., 2002. Astronomically tuned Plio–Pleistocene benthic $\delta^{18}O$ record from South China Sea and Atlantic–Pacific comparison. Earth Planet. Sci. Lett. 203, 1015–1029.

Tiedemann, R., Haug, G.H., 1995. Astronomical calibration of cycle stratigraphy for Site 882 in the northwest Pacific. In: Rea, D.K., Basov, I.A., Scholl, D.W., Allan, J.F. (Eds.), Proc. Ocean Drilling Program, Scientific Results 145, 283–292.

Traverse, A. (2007). Paleopalynology, Second Edition (Topics in Geobiology Vol. 28). Springer: Dordrecht.

Van Nieuwenhove, N., Head, M.J., Limoges, A., Pospelova, V., Mertens, K.N., Matthiessen, J., De Schepper, S., de Vernal, A., Eynaud, F., Londeix, L., Marret, F., Peynaud, A., Radi, T., Rochon, A., 2020. An overview and brief description of common marine organic-walled dinoflagellate cyst taxa occurring in surface sediments of the Northern Hemisphere. Mar. Micropaleontol. 159: 101814, p. 1–46.

Venti, N.L., Billups, K., 2012. Stable-isotope stratigraphy of the northwest Pacific during the Pliocene-Pleistocene climate transition, Palaeogeogr. Palaeoclimatol. Palaeoecol., 326–328, 54–65.

von Stosch, H.V., 1973. Observations on vegetative reproduction and sexual life cycles of two freshwater dinoflagellates, *Gymondinium pseudopalustre* Schiller and *Woloszynskia apiculata* sp. nov. British Phycol. J., 8(2), 105–134.

Warren, B., 1983. Why is no deepwater formed in the North Pacific? J. Mar. Res. 41, 327–347.

Raymo, M.E., Grant, B., Horowitz, M., Rau, G.H., 1996. Mid-Pliocene warmth: stronger greenhouse and stronger conveyor. Mar. Micropaleontol. 27, 313–326.

Venti, N.L., Billups, K., Herbert, T.D., 2017. Paleoproductivity in the northwestern Pacific Ocean during the Pliocene–Pleistocene climate transition (3.0–1.8 Ma). Paleoceanography, 32, 92–103.

Zonneveld, K.A.F., Bockelmann, F., Holzwarth, U., 2007. Selective preservation of organic-walled dinoflagellate cysts as a tool to quantify past net primary production and bottom water oxygen concentrations. Mar. Geol. 237, 109–126.

Zonneveld, K.A.F., Versteegh, G., Kodrans-Nsiah, M., 2008. Preservation and organic chemistry of Late Cenozoic organic-walled dinoflagellate cysts: a review. Mar. Micropaleontol. 68, 179–197.

Zorzi, C.D., 2019. Biostratigraphie des palynomorphes marins dans le Pacifique subarctique au cours du Plio-Pléistocène. Unpublished Ph.D. dissertation, Université du Québec à Montréal.

Zorzi, C., Head, M.J., Matthiessen, J., de Vernal, A., 2019. *Impagidinium detroitense* and *I.*? *diaphanum*: Two new dinoflagellate cyst species from the Pliocene of the North Pacific Ocean, and their biostratigraphic significance. Rev. Palaeobot. Palynol., 264, 24–37.

Zorzi, C., Matthiessen, J., de Vernal, A., 2020. Palynology, biostratigraphy, and paleoceanography of the Plio-Pleistocene at Ocean Drilling Program Site 887, Gulf of Alaska. Palaeogeogr., Palaeoclimatol., Palaeoecol., 546, 109605.

Appendix 1: Plates

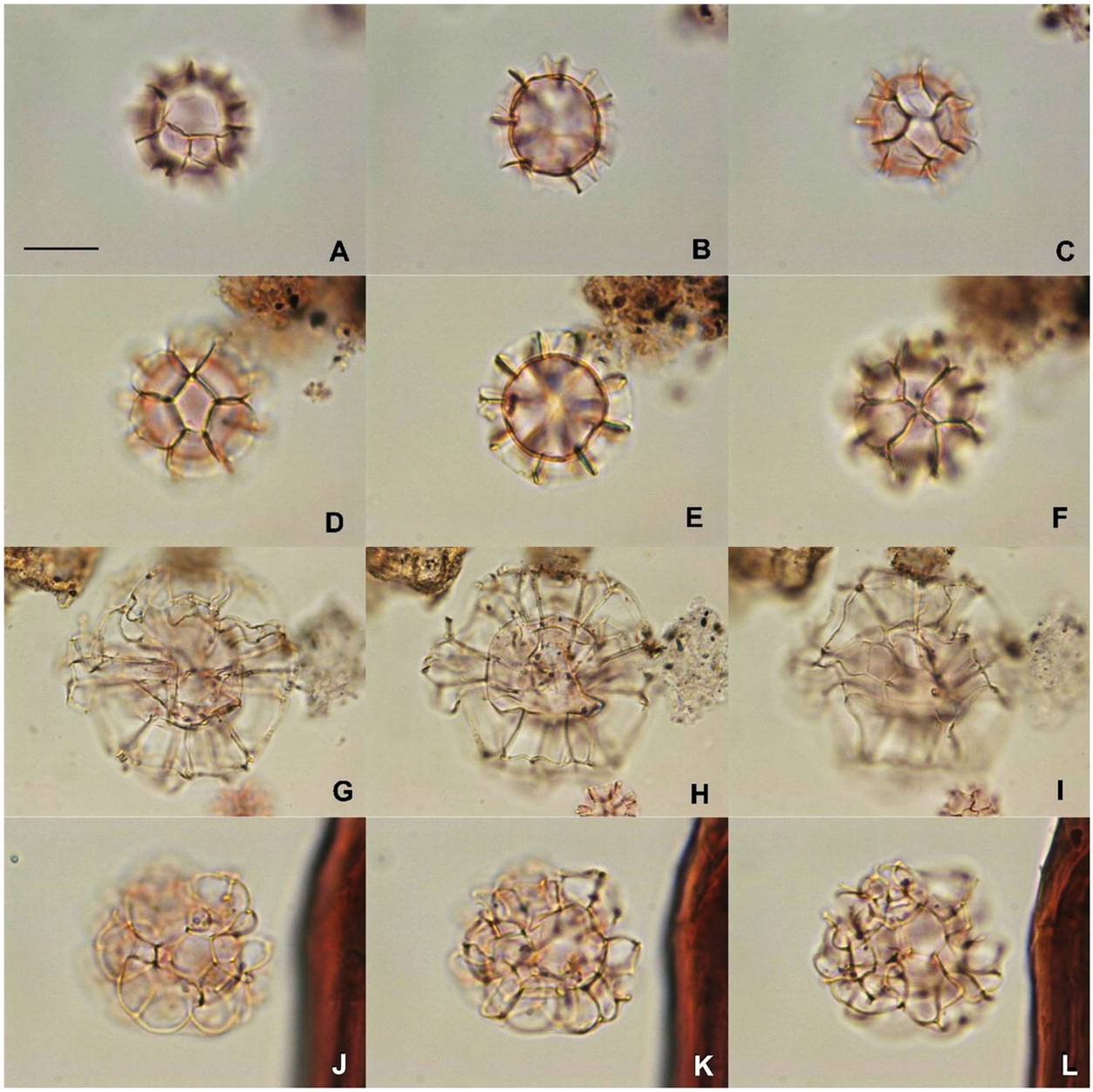

Plate 1

All photos in bright field illumination using x100 oil immersion objective. Scale bar is 20 µm.

A–C. *Cymatiosphaera*? sp.1. Apical view showing A) apical surface with pylome, B) mid-focus, C) antapical surface. Central body maximum diameter 25 µm. Sample 11-1, 84–86 cm; slide 1, England Finder reference N43/4. Age 2517 ka.

D–F. *Cymatiosphaera*? *invaginata* Head et al., 1989. Uncertain view showing D) upper surface, E) mid-focus, F) lower surface. Central body maximum diameter 26 µm. Sample 11-5, 22–24 cm; slide 1; England Finder reference M45/1. Age 22762 ka.

G–I. *Nematosphaeropsis labyrinthus* (Ostenfeld, 1903) Reid, 1974. Apical view of **G**) apical surface, **H**) mid-focus, **I**) antapical surface. Central body maximum diameter 32 µm. Sample 11-6, 54–56 cm; slide 2; England Finder reference G46/2. Age 2706 ka.

J-L. *Cymatiosphaera*? *aegirii* De Schepper and Head, 2014. View uncertain at **J**) upper focus, **K**) mid-focus, **L**) lower focus. Central body maximum diameter 33 µm. Sample 12-2, 51–53 µm; slide 1; England Finder reference J37/0. Age 2759 ka.

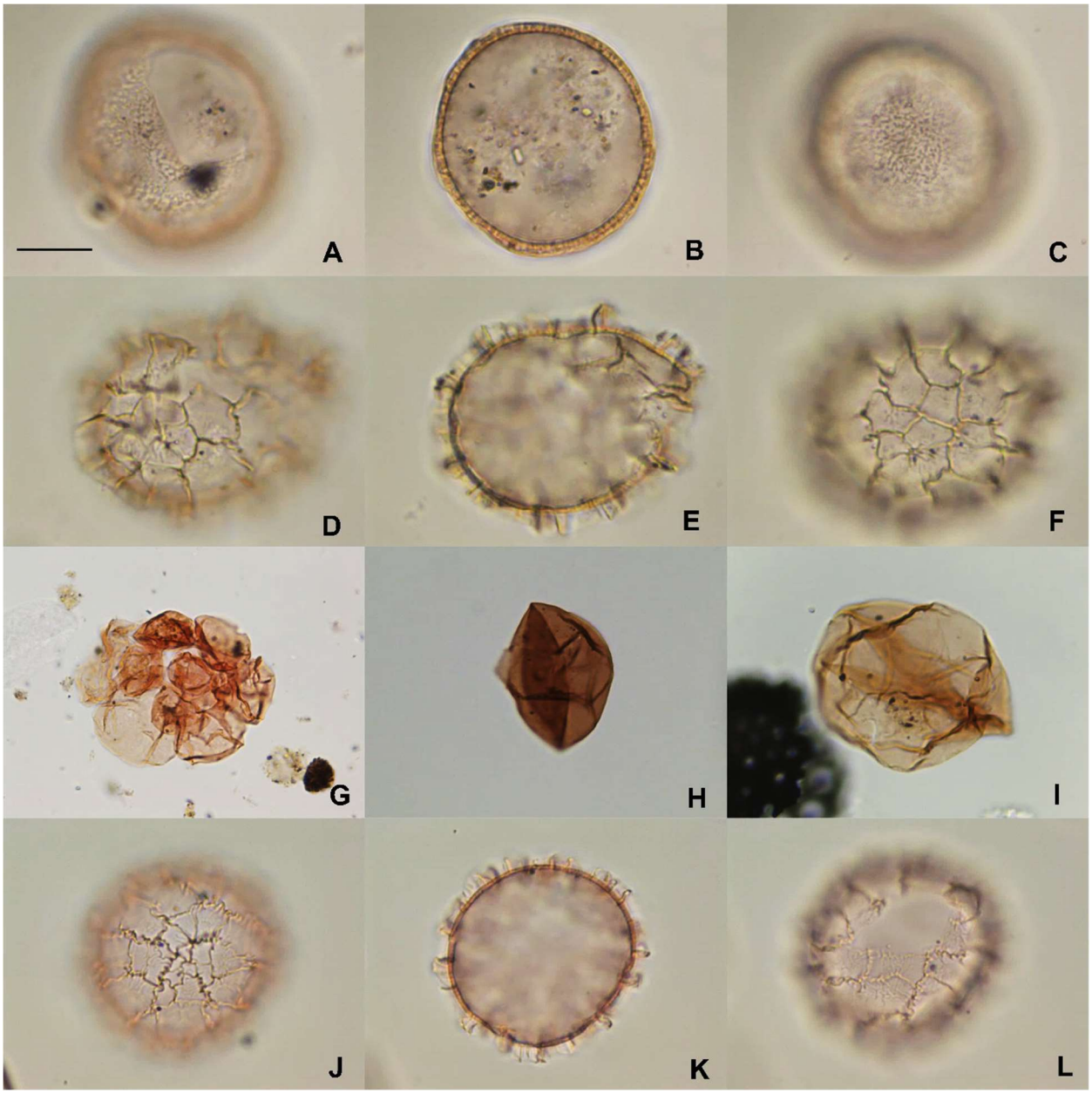
A
B
C
D
E
F
G
H
I
J
K
L

Plate 2

All photos in bright field illumination using x100 oil immersion objective (except where stated). Scale bar represents 20 µm.

A–C. *Habibacysta tectata* Head et al., 1989. Left lateral view of **A**) left lateral surface, **B**) mid-focus, **C**) right lateral surface. Central body maximum diameter 58 µm. Sample 11–5, 146–148 cm; slide 1; England Finder reference E42/4. Age 2696 ka.

D–F. *Pyxidinopsis reticulata* McMinn and Sun, 1994 emend. Marret and de Vernal, 1997. View uncertain of **D**) upper surface, **E**) mid-focus, **F**) lower surface. Central body maximum diameter 64 µm. Sample 11-6, 54–56 cm; slide 1; England finder reference G41/1. Age 2706 ka.

G. Foraminiferal test lining. Maximum diameter 1 µm. Sample 11-1, 45–47 cm; slide 1; England Finder reference D58/1. Age 2497 ka. Photo using 40X objective.

H. *Brigantedinium* sp. (grouped with round brown cysts) lateral? view. Central body flattened. Central body maximum diameter 52 µm. Sample 12-2, 51–53 cm; slide 1; England Finder reference P35/4. Age 2759 ka.

I. *Protoperidinoid* sp. indet. Dorsal? view. Central body flattened. Central body maximum diameter 57 µm. Sample 12-2, 51–53 cm; slide 1; England Finder reference N35/0. Age 2759 ka.

J–L. *Pyxidinopsis reticulata* McMinn and Sun, 1994 emend. Marret and de Vernal, 1997. Ventral view of J) ventral surface, K) mid-focus, L) dorsal surface. Central body maximum diameter 55 µm. Sample 11-2, 88–90 cm; slide 1 England Finder reference M45/1. Age 2574 ka.

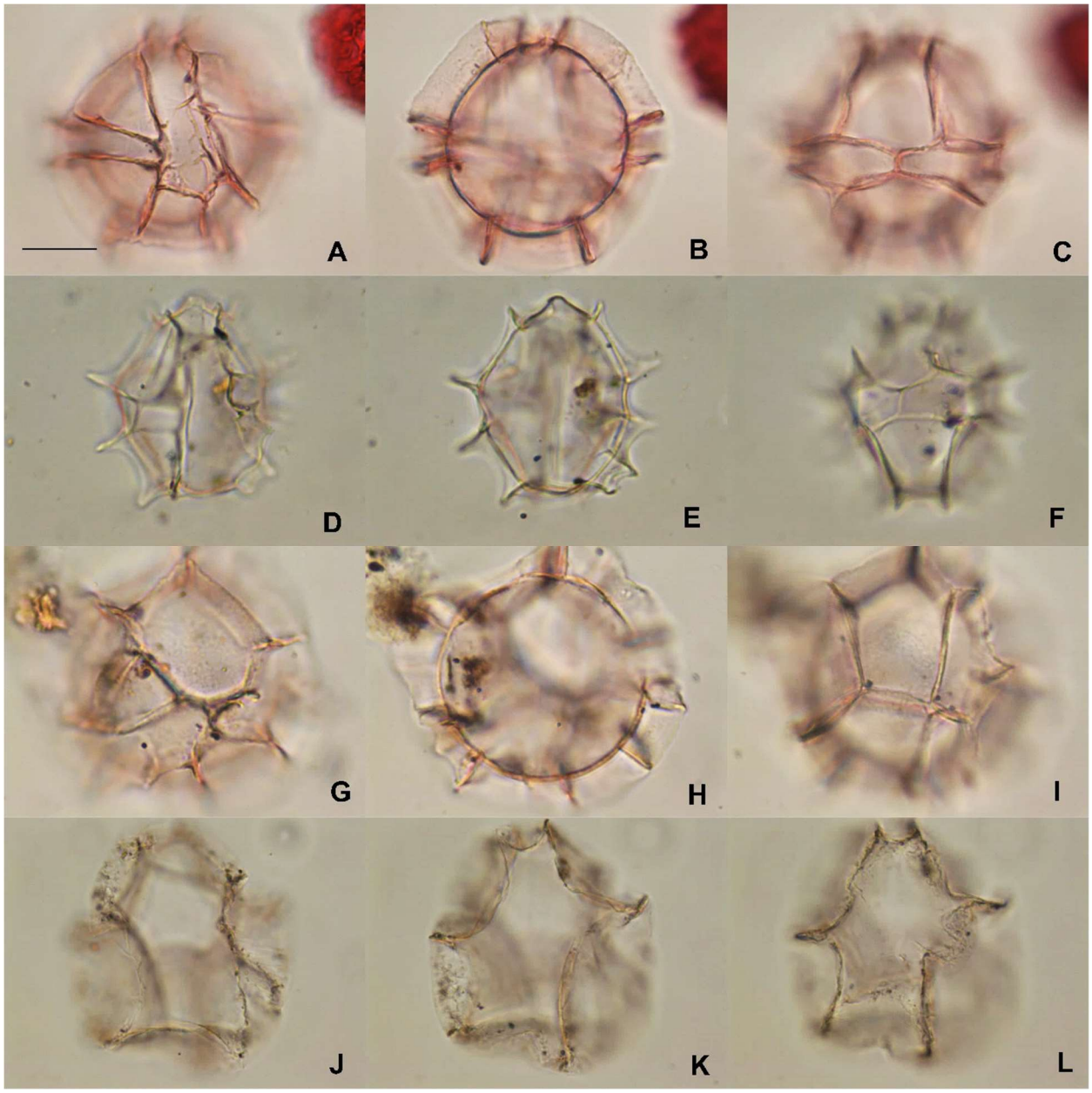
A
B
C
D
E
F
G
H
I
J
K
L

Plate 3

All photos in bright field illumination using x100 oil immersion objective. Scale bar represents 20 µm.

A–C. *Impagidinium* sp. 1. Ventral view of A) ventral surface, B) mid-focus, C) dorsal surface. Central body maximum diameter 50 µm. Sample 11-3, 86–88 cm; slide 1; England Finder reference R65/2. Age 2620 ka.

D–F. *Impagidinium aculeatum* (Wall, 1967) Lentin and Williams, 1981. Ventral view of D) ventral surface, E) mid-focus, F) dorsal surface. Central body maximum diameter 54 µm. Sample 11-3, 33–35 cm; slide 1 England Finder reference S54/2 Age 2601 ka.

G–H. *Impagidinium* sp. 1. View uncertain of **G**) upper surface, **H**) mid-focus, **I**) lower surface. Central body maximum diameter 57 µm. Sample 11-4, 144–146 cm; slide 1 England Finder reference S67/4. Age 2665 ka.

J–L. *Impaginium pallidum* Bujak, 1984. View uncertain at J) upper focus, H) mid-focus, and I) lower focus. Central body maximum diameter 56 µm. Sample 11-4, 104–106 cm; slide 1; England Finder reference M57/1. Age 2652 ka.

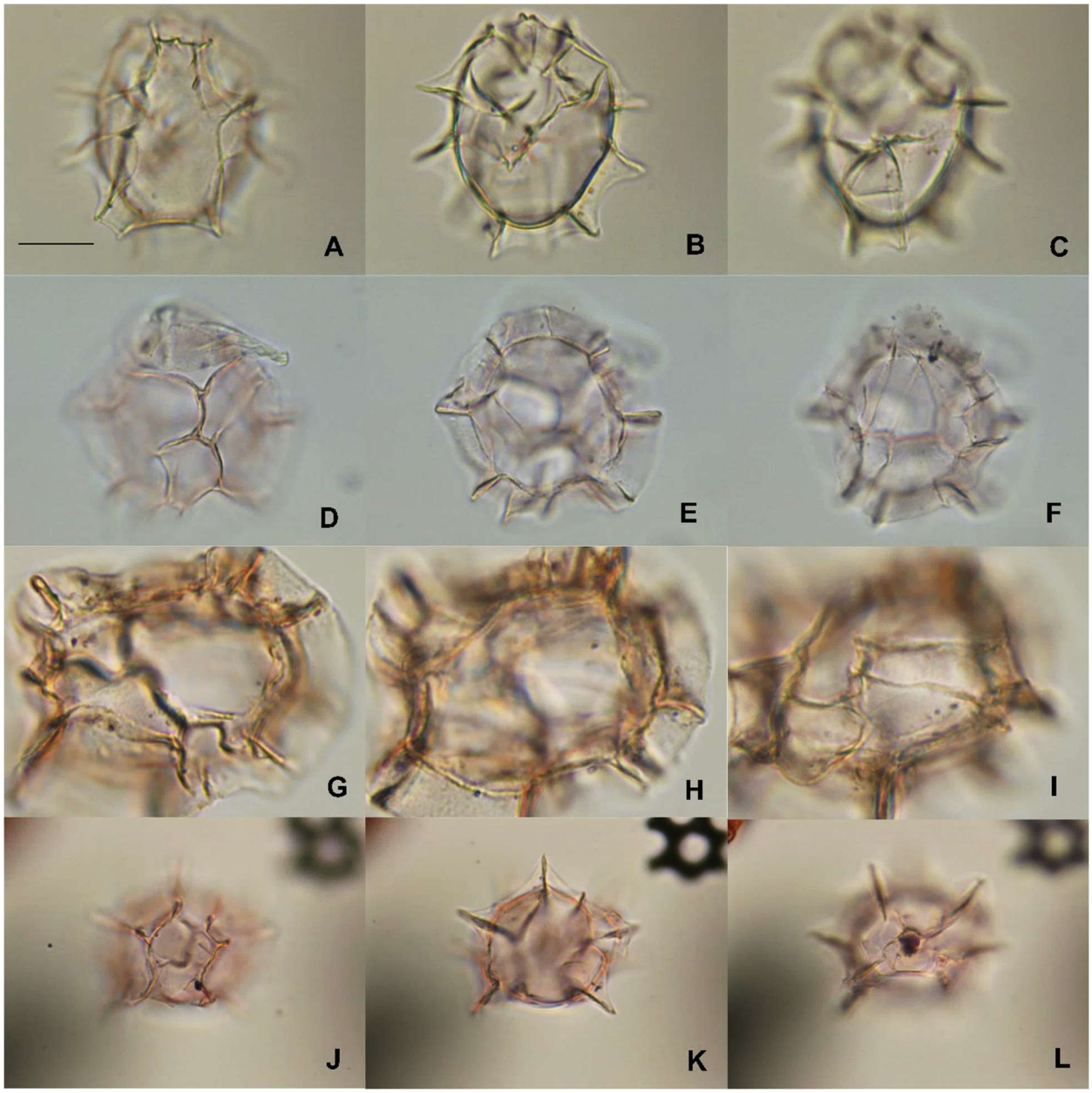
A
B
C
D
E
F
G
H
I
J
K
L

Plate 4

All photos in bright field illumination using x100 oil immersion objective). Scale bar is 20 µm.

A–C. *Impagidinium aculeatum* (Wall, 1967) Lentin and Williams, 1981. Ventral view of **A**) ventral surface, **B**) mid-focus, **C**) dorsal durface. Central body maximum diameter 57 µm. Sample 11-6, 54–56 cm; slide 1; England Finder reference X62/1. Age 2706 ka.

D–F. *Impagidinium* sp. 1. Uncertain view of **D**) upper surface, **E**) mid-focus, **F**) lower focus. Central body maximum diameter 41 µm. Sample 11-2, 74–76 cm; slide 1; England Finder reference T57/1. Age 2570 ka.

G–I. *Impagidinium detroitense* Zorzi et al., 2019. Dorsal view of **G**) dorsal surface, **H**) mid-focus, **I**) ventral surface. Central body maximum diameter 55 µm. Sample 11-1, 146–148 cm. Age 2544 ka. England Finder reference R45/0.

J–L. *Impagidinium aculeatum* (Wall, 1967) Lentin and Williams, 1981. Antapical view of J) antapical surface, K) mid-focus, L) apical surface. Central body maximum diameter 32 µm. Sample 11-6, 54–56 cm; slide 2; England Finder reference F60/4. Age 2706 ka.

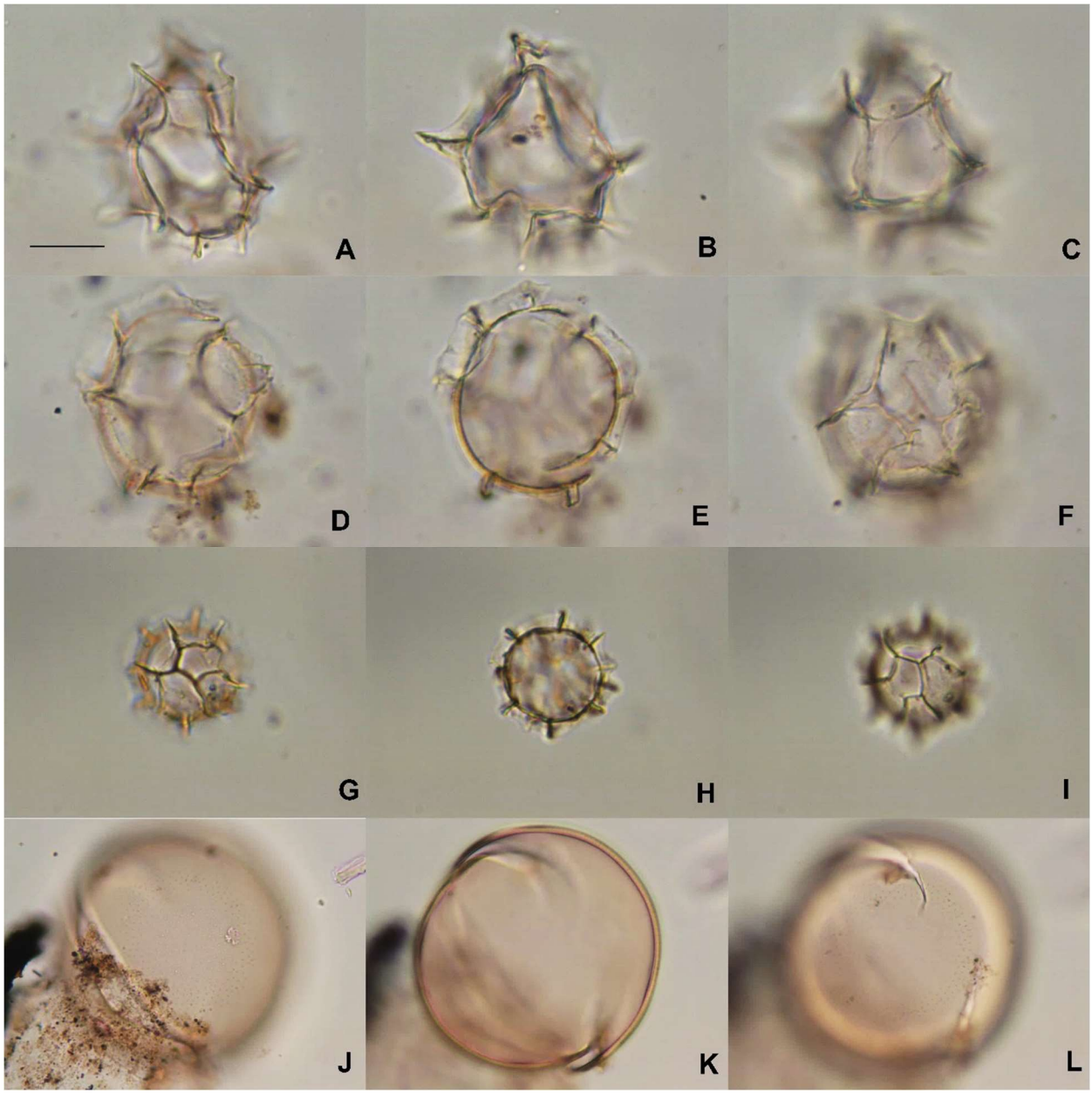
A
B
C
D
E
F
G
H
I
J
K
L

Plate 5

All photos in bright field illumination using x100 oil immersion objective. Scale bar is 20 µm.

A–C. *Impagidinium aculeatum* (Wall, 1967) Lentin and Williams, 1981. Equatorial view of **A**) upper surface, **B**) mid-focus, **C**) lower surface. Central body maximum diameter 41 µm. Sample 11-1, 128–130 cm; slide 1 England Finder reference M42/4. Age 2532 ka.

D–F. *Impagidinium* sp. Uncertain view of **D**) upper surface, **E**) mid-focus, **F**) lower surface. Central body maximum diameter 53 µm. Sample 11-1, 45–47 cm; slide 1 England Finder reference O65/3. Age 2497 ka.

G–I. *Cymatiosphaera* sp. 1. Uncertain view of G) upper surface, H) mid-focus, I) lower surface. Sample 11-3, 17–19 cm; slide 1; England Finder reference K44/0. Age 2596 ka.

J–L. *Tasmanites* sp. Uncertain view of J) upper surface, K) mid-focus, L) lower surface. Central body maximum diameter 69 µm. Sample 12-2, 51–53 cm; slide 1; England Finder reference E65/0. Age 2759 ka.

Appendix 2: Raw counts

Table 1. Processed samples and counted particulate organic material, except *Impagidinium* species.

Samples processed	Age (ka)	Depth (mbsf)	Dried weight (gr)	*Lycopodium clavatum*	Round brown cysts	*Habibacysta tectata*	*Nematosphaeropsis labyrinthus*	*Pyxidinopsis reticulata*	Dinocyst Total	*Cymatiosphaera? invaginata*	*Cymatiosphaera? sp. 1*	*Tasmanites* sp.	Diatom pieces (>10µm)	Woody debris (> 10 µm)	Spores	Pollen	Invertebrate remains
11-1, 45-47	2497	94.77	13	234	300	0	0	10	318	419	0	2	3	183	2	6	21
11-1, 63-65	2506	94.95	17.5	Sample only AOM													
11-1, 84-86	2517	95.16	10.5	270	330	0	0	2	334	120	3	1	17	133	4	6	9
11-1, 101-103	2519	95.33	13.6	298	303	0	0	1	304	132	2	0	8	180	5	2	11
11-1, 114-116	2521	95.46	12.5	254	273	0	0	1	274	330	0	0	2	169	28	13	25
11-1, 128-130	2532	95.6	12.8	195	309	0	0	0	310	141	0	0	395	8	25	14	18
11-1, 146-148	2544	95.78	12.5	356	302	0	1	0	306	363	1	1	477	278	19	5	25
11-2, 4-6	2548	95.86	11.7	122	305	0	0	0	323	321	6	18	115	588	74	21	12
11-2, 21-23	2551	96.03	9.1	256	312	0	0	1	315	83	0	2	11	287	25	17	20
11-2, 44-46	2558	96.26	11.1	297	305	0	0	0	305	112	0	0	85	211	19	8	16
11-2, 62-64	2565	96.44	10.4	275	278	0	0	3	286	21	0	3	24	87	15	0	8
11-2, 74-76	2570	96.56	11.6	370	310	0	1	4	318	37	1	0	28	49	9	3	2
11-2, 88-90	2574	96.7	13.7	325	319	0	2	2	324	29	0	1	48	23	16	14	14
11-2, 101-103	2577	96.82	11	266	313	0	0	3	324	28	2	7	127	535	27	20	27
11-2, 116-118	2580	96.97	9.4	290	319	0	0	1	322	30	3	2	48	358	18	11	16
11-2, 132-134	2585	97.14	8.8	398	286	0	1	0	289	25	4	2	27	255	15	8	17
11-2, 146-148	2589	97.28	8	285	306	0	2	1	313	10	0	2	302	77	13	4	10
11-3, 6-8	2593	97.38	8.7	278	320	0	1	0	321	12	1	0	178	430	26	18	16
11-3, 17-19	2596	97.49	11.2	326	200	0	0	0	200	18	1	0	5	30	2	8	
11-3, 33-35	2601	97.65	14.7	390	86	0	0	2	89	0	0	1	68	17	12	6	3
11-3, 42-44	2605	97.74	11.4	Samples only AOM													
11-3, 62-64	2612	97.94	12.9	Sample only AOM													
11-3, 86-88	2620	98.18	11.7	367	258	0	1	5	264	32	0	0	15	54	12	11	3
11-3, 103-105	2624	98.35	14.4	324	307	0	0	13	323	281	2	3	4	101	8	9	0
11-3, 118-120	2628	98.5	13.3	233	151	0	0	1	154	11	0	1	577	28	2	8	4
11-3, 134-136	2631	98.66	114	300	303	0	0	0	305	21	0	0	623	42	9	3	16
11-4, 0-2	2633	98.82	9.8	355	305	0	0	1	308	21	1	2	203	114	11	9	18

11-4, 7-9	2635	98.89	12.3	344	303	0	0	0	307	37	2	2	17	249	17	19	27
11-4, 33-35	2639	99.15	12.9	390	309	0	1	9	330	320	8	10	488	213	15	12	16
11-4, 52-54	2642	99.34	13.6	365	297	0	0	1	299	150	4	1	396	54	10	5	12
11-4, 63-65	2644	99.45	12.1	402	301	0	0	2	304	152	8	0	411	37	8	10	7
11-4, 82-84	2648	99.64	14.7	447	172	0	1	0	174	70	6	1	153	27	10	13	25
11-4, 104-106	2652	99.86	11.2	367	308	0	0	8	318	63	1	0	115	31	15	6	15
11-4, 122-124	2659	100.04	10.9	341	300	0	5	14	334	251	12	11	28	94	22	18	24
11-4, 144-146	2665	100.26	9.9	288	403	0	2	7	420	360	21	6	255	84	19	7	18
11-5, 2-4	2669	100.34	15.8	365	315	0	4	18	346	580	41	5	847	389	28	21	26
11-5, 22-24	2673	100.54	13.4	332	303	0	3	16	336	632	76	13	478	362	16	8	22
11-5, 36-38	2676	100.68	13.9	387	302	0	0	6	316	432	27	8	404	250	12	21	17
11-5, 47-49	2678	100.79	10.8	345	305	0	1	4	312	433	17	0	368	102	8	52	29
11-5, 67-69	2682	100.99	12.1	387	307	0	0	4	319	390	16	8	420	78	16	18	18
11-5, 91-93	2686	101.23	15.7	359	308	0	0	5	313	162	21	0	427	45	12	7	27
11-5, 114-116	2690	101.46	16.1	376	300	0	0	9	310	85	25	0	393	37	8	5	16
11-5, 132-134	2694	101.64	17.6	Sample only AOM													
11-5, 146-148	2696	101.78	18.6	397	116	34	18	21	197	0	0	0	348	31	4	8	28
11-6, 4-6	2698	101.86	12.9	384	270	11	22	31	346	3	0		214	23	7	2	48
11-6, 22-24	2701	102.04	11.6	400	81	0	1	11	95	6	0	0	437	37	2	0	25
11-6, 35-37	2703	1102.17	12	355	305	0	4	7	335	338	21	17	266	42	16	11	30
11-6, 54-56	2706	102.36	11	389	306	0	6	2	325	355	19	10	512	37	10	17	24
11-6, 67-69	2710	102.49	9.9	464	300	0	4	0	318	689	31	9	106	35	24	26	
11-6, 97-99	2715	102.79	15.2	432	306	0	1	0	314	622	22	6	214	26	18	17	46
11-6, 112-114	2718	102.94	14.5	552	319	0	3	1	328	645	2	1	587	31	16	5	53
11-6, 125-127	2720	103.07	14.2	511	269	0	0	2	283	624	0	0	545	27	12	8	26
11-6, 142-144	2721	103.24	12.1	489	295	0	1	1	305	635	3	0	556	38	15	16	38
11-7, 6-8	2726	103.38	17.3	422	310	0	0	2	313	533	2	1	424	28	18	19	36
11-7, 23-25	2730	103.55	16.8	421	309	0	1	8	328	479	4	8	407	36	27	25	62
11-7, 46-48	2731	103.78	11.7	402	320	0	0	2	326	387	6	4	288	21	17	15	58
11-7, 61-63	2732	103.93	16	388	300	0	1	5	317	366	3	10	275	39	21	28	74
12-1, 0-2	2736	103.95	14.5	390	308	0	1	11	328	358	10	6	376	41	16	19	89
12-1, 16-18	2741	103.98	11.6	429	299	0	2	6	310	378	7	3	534	30	16	14	18
12-1, 32-34	2743	104.14	12.7	452	308	0	0	8	326	413	16	8	316	42	18	27	27
12-1, 48-50	2744	104.3	13.2	386	301	0	0	12	335	403	13	21	179	19	24	28	15
12-1, 64-66	2746	104.46	17.7	411	296	0	0	8	321	377	10	17	68	28	28	22	19
12-1, 77-79	2747	104.59	12.1	460	309	0	0	7	331	311	3	13	384	21	26	17	13
12-1, 96-98	2749	104.78	15.5	427	301	0	0	0	309	421	9	5	277	36	15	10	22

12-1, 112-114	2750	104.94	14.3	386	303	0	3	2	328	210	6	15	463	27	21	16	21
12-1, 128-130	2751	104.1	13	388	299	0	6	0	322	437	13	9	273	39	32	19	29
12-1, 144-146	2752	105.26	10.8	447	308	0	4	0	330	320	3	4	276	36	34	18	18
12-2, 2-4	2753	105.34	9.7	395	300	0	17	0	331	392	2	4	290	20	22	9	17
12-2, 18-20	2756	105.5	9.9	484	298	0	8	6	325	384	8	2	248	42	27	23	28
12-2, 34-36	2757	105.66	12	421	300	0	7	7	322	451	2	0	79	33	14	10	21
12-2, 51-53	2759	105.83	9	411	309	0	0	0	316	488	17	5	109	48	28	22	14
12-2, 66-68	2761	105.98	12.7	486	311	0	0	14	344	513	19	18	102	57	31	27	17

Table 2. *Impagidinium* species raw count.

Samples processed	**Age (ka)**	**Depth (mbsf)**	**Dried weight (gr)**	***Impagidinium* sp.**	***Impagidinium aculeatum***	***Impagidinium patulum***	***Impagidinium sphaericum***	***Impagidinium detrioitense***	***Impagidinium japonicum***	***Impagidinium pallidum***	***Impagidinium* spp. total**	**Dinocyst total**
11-1, 45-47	2497	94.77	13	5	0	1	0	0	0	0	6	318
11-1, 63-65	2506	94.95	17.5	Sample only AOM								
11-1, 84-86	2517	95.16	10.5	1	0	0	0	0	0	0	1	334
11-1, 101-103	2519	95.33	13.6	0	0	0	0	0	0	0	0	304
11-1, 114-116	2521	95.46	12.5	0	0	0	0	0	0	0	0	274
11-1, 128-130	2532	95.6	12.8	0	1	0	0	0	0	0	1	310
11-1, 146-148	2544	95.78	12.5	2	0	0	0	1	0	0	2	306
11-2, 4-6	2548	95.86	11.7	0	0	0	0	0	0	0	0	323
11-2, 21-23	2551	96.03	9.1	0	0	0	0	0	0	0	0	315
11-2, 44-46	2558	96.26	11.1	0	0	0	0	0	0	0	0	305
11-2, 62-64	2565	96.44	10.4	0	1	0	1	0	0	0	2	286
11-2, 74-76	2570	96.56	11.6	0	2	0	1	0	0	0	3	318
11-2, 88-90	2574	96.7	13.7	0	0	0	0	0	0	0	0	324
11-2, 101-103	2577	96.82	11	1	0	0	0	0	0	0	1	324
11-2, 116-118	2580	96.97	9.4	0	0	0	0	0	0	0	0	322
11-2, 132-134	2585	97.14	8.8	0	0	0	0	0	0	0	0	289
11-2, 146-148	2589	97.28	8	2	0	0	1	0	0	0	3	313
11-3, 6-8	2593	97.38	8.7	0	0	0	0	0	0	0	0	321
11-3, 17-19	2596	97.49	11.2	0	0	0	0	0	0	0	0	200
11-3, 33-35	2601	97.65	14.7	0	0	0	0	0	0	0	0	89
11-3, 42-44	2605	97.74	11.4	Sample only AOM								

11-3, 62-64	2612	97.94	12.9	Sample only AOM								
11-3, 86-88	2620	98.18	11.7	0	0	0	0	0	0	0	0	264
11-3, 103-105	2624	98.35	14.4	0	0	0	0	0	0	0	0	323
11-3, 118-120	2628	98.5	13.3	0	0	1	0	0	0	0	1	154
11-3, 134-136	2631	98.66	114	1	0	0	0	0	0	0	2	305
11-4, 0-2	2633	98.82	9.8	0	0	0	0	0	0	0	0	308
11-4, 7-9	2635	98.89	12.3	0	0	2	0	0	0	0	2	307
11-4, 33-35	2639	99.15	12.9	0	0	1	0	0	0	0	1	330
11-4, 52-54	2642	99.34	13.6	0	0	0	0	0	0	0	0	299
11-4, 63-65	2644	99.45	12.1	1	0	0	0	0	0	0	1	304
11-4, 82-84	2648	99.64	14.7	0	0	0	0	0	0	0	0	174
11-4, 104-106	2652	99.86	11.2	1	0	0	0	0	0	2	3	318
11-4, 122-124	2659	100.04	10.9	0	0	2	2	0	0	0	4	334
11-4, 144-146	2665	100.26	9.9	0	0	0	2	0	0	0	2	420
11-5, 2-4	2669	100.34	15.8	1	0	1	1	0	0	1	4	346
11-5, 22-24	2673	100.54	13.4	1	0	0	0	0	0	0	1	336
11-5, 36-38	2676	100.68	13.9	0	0	0	0	0	0	0	0	316
11-5, 47-49	2678	100.79	10.8	2	0	0	0	0	0	0	2	312
11-5, 67-69	2682	100.99	12.1	0	0	0	0	0	0	0	0	319
11-5, 91-93	2686	101.23	15.7	0	0	0	0	0	0	0	0	313
11-5, 114-116	2690	101.46	16.1	1	0	0	0	0	0	0	1	310
11-5, 132-134	2694	101.64	17.6	Sample only AOM								
11-5, 146-148	2696	101.78	18.6	9	0	0	0	0	0	8	9	197
11-6, 4-6	2698	101.86	12.9	0	0	1	0	0	1	12	13	346
11-6, 22-24	2701	102.04	11.6	0	0	0	0	0	0	2	2	95
11-6, 35-37	2703	1102.17	12	2	0	0	0	0	0	0	2	335
11-6, 54-56	2706	102.36	11	0	0	1	0	0	0	0	1	325
11-6, 67-69	2710	102.49	9.9	1	0	0	0	0	0	4	5	318
11-6, 97-99	2715	102.79	15.2	0	0	0	0	0	0	1	1	314
11-6, 112-114	2718	102.94	14.5	0	4	0	0	0	0	3	4	328
11-6, 125-127	2720	103.07	14.2	0	4	0	0	0	0	8	12	283
11-6, 142-144	2721	103.24	12.1	1	0	0	0	0	0	8	9	305
11-7, 6-8	2726	103.38	17.3	0	0	0	0	0	0	0	0	313
11-7, 23-25	2730	103.55	16.8	0	0	0	0	0	0	2	2	328
11-7, 46-48	2731	103.78	11.7	0	0	0	0	0	0	0	0	326
11-7, 61-63	2732	103.93	16	0	0	0	0	0	0	1	1	317
12-1, 0-2	2736	103.95	14.5	0	0	0	0	0	0	2	2	328
12-1, 16-18	2741	103.98	11.6	0	0	0	0	0	0	0	0	310
12-1, 32-34	2743	104.14	12.7	1	0	0	0	0	0	1	2	326
12-1, 48-50	2744	104.3	13.2	1	0	0	0	0	0	0	1	335
12-1, 64-66	2746	104.46	17.7	0	0	0	0	0	0	0	0	321
12-1, 77-79	2747	104.59	12.1	1	0	0	0	0	0	2	3	331

12-1, 96-98	2749	104.78	15.5	0	0	0	0	0	0	3	3	309
12-1, 112-114	2750	104.94	14.3	1	0	0	0	0	0	4	5	328
12-1, 128-130	2751	104.1	13	0	0	0	0	0	0	8	8	322
12-1, 144-146	2752	105.26	10.8	0	0	0	0	0	0	14	14	330
12-2, 2-4	2753	105.34	9.7	0	0	0	0	0	0	10	10	331
12-2, 18-20	2756	105.5	9.9	0	0	0	0	0	0	11	11	325
12-2, 34-36	2757	105.66	12	3	0	0	0	0	0	8	8	322
12-2, 51-53	2759	105.83	9	0	0	0	0	0	0	2	2	316
12-2, 66-68	2761	105.98	12.7	0	0	0	0	0	0	1	1	344

Appendix 3: Standard palynological processing at Brock University used in this study

By M.J. Head, 2020

Protocol for processing palynological samples:

This method of processing is based on "standard procedures" but emphasizes three crucial objectives:

i) Personal safety – always use HF-rated gloves when putting your hands in the fume hood, and be aware that even dilute HF can be extremely toxic. Always look out for drops of spilt HF and neutralize them using a solution of sodium carbonate which should be present in a container in the fume hood. Always decontaminate gloves by dipping gloved hands in the container of sodium carbonate before removing hands from fume hood. When using HF, the following clothing is required: lab coat and underclothing that fully covers the legs, acid-resistant apron, visor to protect face, HF-rated gloves (neoprene rubber is best [nitrile not recommended for conc. ≥30%]), and shoes that fully cover the feet. Waste HF must be stored for later disposal, never washed down the sink. Only use HF when you have had the requisite training, and always let someone nearby know when you are planning to use HF. Make sure you know what to do in the event of an incident with HF. Remember that weak HF burns may not produce symptoms for up to 24 hours. A tube of 2.5% calcium glauconate gel should be available in the lab, and another kept at in the fridge at home (expires after 1 year). Note the location of the safety shower and eyewash station.

Liquified phenol (used to prevent microbial growth in palynological residues) is likewise very toxic and absorbed through the skin. It must only be handled using gloves. We now use a saturated solution of thymol rather than liquified phenol because it is less toxic.

ii) Contamination – we aim to reduce the possibility of contamination between samples and residues to very nearly zero. In dinoflagellate cyst studies, even one specimen in an assemblage of thousands can have biostratigraphic / evolutionary significance. We MUST therefore be able to trust that this rare specimen is not a contaminant from another sample in the lab. Care is especially important in a multi-user environment. Residues in water can travel in air via splashing and spray that lead to aerosols, and by airborne suspension if they become dry. Make sure adjacent sample containers are always covered! Always use imagination when processing in the lab to minimize the risk of contamination.

iii) Residue loss and biasing – Always be careful when decanting residue, as this can lead to loss of residue (a problem with samples that are lean) and bias owing to the finer fraction (smaller species including small acritarchs) being more readily lost. This can lead to biased counts and wrong paleoenvironmental interpretations.

Step-by-step guide to processing for marine palynology:

1. Wash 400 ml Nalgene Griffin polypropylene beakers, low form, in preparation for sample processing. First, soak in warm soapy water, then clean vigorously with a soft, non-abrasive cloth using non-abrasive soap. Clean with hot tap water and rinse thoroughly with distilled water to

remove any tap water (which in the St. Catharines area comes from the Decew Falls Water Treatment Plant on a reservoir complex that includes lakes Moody and Gibson, adjacent to Brock University). The St Catharines tap water is likely to be contaminated with aquatic palynomorphs. A piece of parafilm is placed over the beaker to prevent airborne contamination prior to and during processing.

2. When the beakers are dry, remove any existing external markings with solvent. Using an indelible marker, number each beaker with a designated lab number (keeping the numbering simple, e.g. your initials plus 1 to 24 [e.g. MH 1, MH 2 etc.) in two places: high on one side and low on the opposite side (as a precaution). Write this number also on the sample bag to correlate the sample number with the lab number. Note also in lab note book.

3. Clean samples prior to further processing. In the case of DSDP, ODP, IODP cores, these have been stored in damp conditions in their original core liner that has been split length-wise into two halves, the "archive half" and the "working half", which have a "D" cross section. The core surfaces will acquire fungal growth over time, both on the upper flat surface and the curved surface touching the core liner itself. We clean samples on a square of aluminum foil, with new foil used for each sample.

The samples we receive from IODP have been collected almost always from the working half. Each sample must be trimmed with a spatula or knife to remove flat and curved surfaces where fungal contamination may exist. If it is not removed now, the fungal hyphae will persist through processing and cause clumping of the palynological residues. It is usually enough to remove the

upper 1 or 2 mm of the surface. Most important to clean hands and knife / spatula between samples so as not to cross-contaminate them.

4. Gently crush the cleaned sediment sample in aluminum foil using a hammer and steel plate, wrapping the foil around the sample so that the sample is contained securely within the foil. If the sediment is soft, it can be broken into pieces with the fingers, being sure to wash the fingers between samples. The pieces of sediment should be pea sized to accelerate drying and acid penetration.

5. Place an empty paper "cup cake" liner (used for baking cup cakes) onto the cleaned weighing plate of an electronic balance. Zero the balance. Remove empty baking cup. Mark sample number on the baking cup. Transfer crushed sample into the baking cup, and weigh the sediment. Because the balance has been zeroed with an empty baking cup, it will now be weighing only the sediment. Note the sample weight in grams to one decimal place. We generally aim for up to 20 grams for each sample prior to drying.

6. Place each weighed sample in its numbered paper baking cup on a baking tray. We process 24 samples at a time, so 24 samples in their baking cups should be on the baking tray. Cover the samples with several sheets from a roll of kitchen toweling. This prevents dust and other contaminants from setting onto the samples. Place the covered baking tray in a low-temperature oven for ~24 hours at around 40°C. This will completely dry the samples without actually baking

them or thermally altering the organics. The samples can lose 30% or more of their weight during drying.

7. Remove samples on baking tray from oven and re-weigh them on the electronic balance, zeroing as before to remove the weight of the baking cup. The samples may have lost a third of their weight. The dry weight of the sample is more important than the wet weight, because it is the dry weight we use for expressing cyst concentration in the sediment (n cysts /gram dry weight).

8. Transfer dried and weighed sediment from baking cup into a clean, numbered, 400 ml beaker, ensuring that the sample is tipped gently onto the bottom of the beaker to prevent a cloud of dust from forming. Dispose of empty baking cup. Re-seal beaker with Parafilm.

9. When all samples have been weighed and placed in beakers, the beakers are transferred to the fume hood and small amounts of 20% of concentrated room-temperature HCl are added in turn to each sample. Our concentrated HCl is 38%, so 20% of concentrated is actually 7.6%. It is important to add the acid initially in small increments to avoid any possibility of bubbling over. Gradually add up to 200 ml of acid to each beaker, swirling the sediment into suspension several times, and allow to stand overnight to dissolve all carbonates. Make sure that the Parafilm is securely attached to the top of the beaker. Do not add more than 200 ml of acid or you will not be able to effectively swirl, i.e., create a vortex sufficient to move the sediment into suspension. Do not expose the residues for much more than about 12 hours because HCl will damage some protoperidiniacean cysts over time.

10. After standing overnight, swirl the sediment into suspension and add distilled water vigorously up to about 500 ml. Allow to stand for about 9 hours. Then vibrate the beaker by dragging briefly and by abrupt short twisting movements to flocculate any fine material adhering to the sides of the beaker as the result of electrostatic forces. Allow 3 more hours for this flocculant to settle.

11. Rinse a glass pipette with distilled water and connect it to the hose attached to the side of the siphon (which is attached to the tap/faucet). Then open the tap/faucet and allow water to run to produce suction (Venturi effect) through the pipette.

12. Carefully place the beaker next to the tap avoiding any abrupt movement or twisting that could bring sediment back into suspension; open the Parafilm cover and insert the pipette to suck the supernatant. While removing this supernatant, prevent the pipette from contacting the sides of the beaker to minimize the risk of contamination. Slowly begin tilting the beaker when the liquid reaches around 150 mL. This helps to prevent the tip of the pipette from getting too close to the sediment in the bottom. Remove the pipette when reaching the lowest safe level of supernatant to avoid any chance of losing sediment. Re-seal beaker with Parafilm.

13. Rinse the tip of the pipette with tap water and allow re-circulation (tap water being sucked through the pipette), then repeat using distilled water. Keep the tap water running at all times to maintain the suction and prevent tap water back-flowing into the hose connected to the pipette.

14. Transfer the beaker to the fume hood and swirl the sediment back into suspension. Add distilled water vigorously up to 500 mL and allow to stand for 9 hours. Subsequently, repeat the procedure for flocculation mentioned in step 10.

15. Repeat steps 10 to 13 (siphoning off and refilling with distilled water) until samples reach a pH of about 6 (pH of distilled water). When measuring the acidity, use one end of the pH paper to test the sample and add a small amount of distilled water on the other end for comparison. When a pH of 6 is reached, then siphon off the supernatant as before. There will usually be around 75 to 100 ml of sediment and water at the bottom of the beaker.

16. Swirl the sediment into suspension, and add conc. room-temperature HF until it reaches the 200 mL mark (we use HF at a concentration of around 38%, commercial grade, not analytical grade which is unnecessarily pure and expensive). Don't go higher than the 200 mL mark, because it will otherwise be difficult to swirl the sample effectively (a vortex needs to be created when swirling to bring all the sediment into suspension and thoroughly mix the HF.

Due to the hazardous nature of this acid, is essential to wear all available safety protection (lab coat, HF-rated apron, HF-rated gloves, mask, shoes that fully cover the feet, etc.) when using it. Look for any drips at all times. If there is a suspicion of drips, rinse the affected area(s) with a sodium carbonate solution using a cloth. Also, dip gloves in this solution always before removing them from the fumehood. Indeed, anything that may have been in contact with the HF must be immersed in the sodium carbonate bath before its removal from the fume hood.

17. Swirl the sediment into suspension 3 times a day for 5 days. This is essential because the HF otherwise stratifies at the bottom of the beaker and will stop reacting with the sediment. Note that HF is not a strong acid in spite of its extreme toxicity.

18. Twist and drag the beakers to produce flocculation of particles in the sides of the beaker. Allow to stand for three hours.

19. Peel back the Parafilm cover from the beaker. Make sure to avoid the drops condensed on its inner side since they could contain HF. Begin decanting the HF from the samples to a 1 L beaker by slow tilting to avoid any abrupt movement of the sediment that could bring it into suspension. Reverse the tilt slowly if the sediment at the bottom of the beaker begins to cascade. Stop decanting if there is any chance of losing organic residue. Label a plastic bottle with "Waste HF" and then transfer the content of the 1 L beaker to this bottle. It is important not to accumulate too much HF in the 1 L beaker. Hence, it is recommended that the decanted acid be transferred to the waste HF bottle after every two or three samples. Note that the reason we do not use any abrasive to clean the insides of the beakers (we use warm water, non-abrasive soap, and a soft cloth) is that if they retain their unscratched shiny inner surface, the easier it is to decant from them – as the beaker is tilted the sediment slides gradually along the bottom with less chance of cascading into suspension. When decanting, always decant towards you so you are looking closely and directly into the beaker. This way you will be able to see if the sediment is beginning to cascade into suspension.

20. After decanting, swirl beakers to bring the residue into suspension and add distilled water up to around 500 mL and allow to stand overnight.

21. The next morning, decant carefully, then repeat steps 19 and 20 until the supernatant is neutral (pH 6 if using distilled water).

22. Using an indelible felt-tip pen, label 50 mL screw-top disposable plastic conical test tubes with the same designated lab number used in the beakers. Label in two different places: high on one side and low on the opposite side. Also label the screw top.

23. Decant the supernatant from the beaker, and transfer the residue to a 50 mL test tube. Make sure the number in the test tube matches the number on the beaker. The residue may not all fit into the test tube. If that is the case, spin down in a centrifuge, decant the supernatant, and continue to transfer residue into the 50 mL test tube. Repeat until all the residue is transferred to the test tube.

24. Decant the supernatant. Use a vortex mixer to ensure the residue is fully mixed, but be careful always try to make sure the residue does not reach the cap. Also important to check that there is no plug of consolidated residue at the bottom of the test tube. When fully mixed, add about 40 mL of HCl (20% of concentrated, as in step 9) to the test tubes and allow stand for half a day. This helps to remove any precipitates formed during HF treatment. Then fill the tubes with distilled water, and spin down in a centrifuge.

25. For the centrifuge, set the RPM at 3500 and spin the test tubes for 3 minutes, then decant the supernatant. Repeat until reaching a pH of 6, this being the pH of distilled water. Between centrifuge steps, decant, mix with the vortex mixer, add water, centrifuge etc.

26. When the residue is neutral, it is decanted and vortex mixed so as to be completely in suspension. The desired number of Lycopodium clavatum tablets (usually around 1 to 3 per 10 grams of dry sediment, but see below) are added to each sample. They dissolve in HCl, so can be added directly to the residue with a squirt of HCl. However, one cannot always guarantee that the tablets have dissolved (and they may be concealed by the black organic residue). Therefore we usually dissolve the tablets in separate 15-mL plastic disposable test tubes with a brief squirt of HCl, and then wash the dissolved tablets into the tubes containing the residues carefully to ensure all the spores have been transferred. The residue is then vortex mixed until the residue and Lycopodium clavatum spores are fully mixed with the residue. Ensure that there is no plug of consolidated residue at the bottom of the test tube.

A note on the number of Lycopodium clavatum tablets to use. Ideally, you want to aim for a dinocyst : L. clavatum spore ratio of about 1:1 to obtain the smallest error on your calculations for the most efficient use of your time. It doesn't help much to calculate that your concentration for a particular sample is say 5000 cysts/ gram, only to discover that the error is +/- 20,000 cysts/gram because there were too few L. clavatum spores to count in your slides! See Louis J. Maher, Jr. (1981, Review of Palaeobotany and Palynology 32, 153–191) for details. But knowing how many Lycopodium clavatum tablets to add requires knowing the dinocyst concentration in advance, which is the very information you are aiming to find out. So, estimate the dinocyst concentration you expect in your samples by consulting previous studies of dinocysts under similar settings. See also Appendix 3.

27. To remove HCl added in step 26, spin down the samples using the same parameters mentioned in step 25. Then, remove approximately 3/4 of the supernatant and mix the residue using the vortex mixer being careful always to bring all the residue into suspension. When mixing on the vortex mixer, important to prevent the contents from making contact with the screw cap of the centrifuge tube. If this does happen, use distilled water from a squirt bottle to wash the residue from the screw cap back into the centrifuge tube.

28. Prepare the sieve holder by washing carefully the plastic tube and the plastic collar with warm soapy water and a plastic scouring pad. Rinse with distilled water, and place on a watch glass that has similarly been cleaned and rinsed in distilled water. Place a square of pre-cut 10 µm sieving mesh on the plastic tube and then place the collar over the mesh and press down to secure the sieving mesh to the sieve. The sieve is now ready for use. Place a second cleaned watch glass over the sieve to prevent dust particles from entering it.

29. Prepare a disposable glass pipette by first labeling it with the unique sample number using an indelible marker. Then rinse the pipette using a squirt bottle with distilled water. Place a bulb on the glass pipette. The pipette is now ready for use.

30. Move the sieve on its watch glass over to the sink. Rinse out the sieve using a jet of distilled water from the squirt bottle.

31. Now use the pipette to complete the homogenization of the residue (step 27) by effecting a squirting/sucking motion with the pipette. This homogenization is essential to ensure that the Lycopodium spores are thoroughly mixed with the palynomorphs of the sample. Immediately

after homogenization, fill the pipette with suspended residue from the 50 ml centrifuge tube. Place this residue in the sieve. Add distilled water from the squirt bottle until the sieve is ¾ full. Lift up the sieve holder with one hand, and rapidly tap the collar of the sieve holder with a finger nail from the other hand. The vibration will assist in the sieving. While sieving, tilt and rotate the sieve and use the jet from the squirt bottle to help clean the sieve surface and prevent the pores from getting clogged. Continue to add more distilled water from the squirt bottle, and continue sieving until the the filtrate is clear. This sieving operation is conducted over the sink to avoid a mess. The filtrate is not saved. Depending on how much of the residue goes through the sieve, it is often advisable to introduce one or two additional pipettes of residue into the sieve, in order to have sufficient sieved residue for at least two microscope slides.

32. Rinse pipette to remove any unsieved residue. Extract a minute amount of the sieved residue from the sieve using the pipette, and place this small fraction of a drop onto a microscope slide. Examine the wet preparation ("wet prep") under the microscope to determine if any further treatment of the residue (e.g. brief ultrasound, warming in calgon) is needed. The residue is then rinsed off the microscope slide (it is not saved, which is why a very small quantity is used). Check that there are sufficient Lycopodium spores relative to dinocysts. There is still time to add additional Lycopodium tablets if needed.

33. Using an indelible marker pen, label a disposable 15 mL screwtop centrifuge tube with its laboratory sample code. And then rinse using distilled water to remove any factory contamination (microscopic pieces of plastic etc.). As for the 50 ml tubes, label twice (high on

one side and low on the other to minimize the risk of accidental deletion which would then render the sample useless). Label the plastic cap as well as the tube itself.

34. Place the 15 mL tube in a centrifuge rack next to the sink, and overhanging the sink. Transfer the residue from the sieve into the 15 mL tube using a bent-tipped squirt / squeeze bottle with a fine spray. Excess water will drain into the sink. Then slightly loosen the sieve collar. This will release residue trapped between the sieve material and the base of the sieve tube. Squirt again to remove this residue into the 15 mL tube. Try to get all the residue into the 15 ml tube. If you are not, you will need to spin down the 15 mL tube in the centrifuge, pipette off the supernatant, and transfer the remaining residue to the centrifuge tube. N.B. When using squeeze bottle, do not put the nozzle into the sieve holder as this will risk contaminating the tip of the nozzle with residue that could then be transferred to the next sample.

35. Spin down the 15 mL tube in the centrifuge (we use 3500 rpm for 3 mins, but times will vary depending on the diameter of the rotor in the centrifuge). Then pipette off the supernatant carefully to within about 4–5 mL of the base. If step 32 showed there was no need for further treatment, then mix in vortex mixer to homogenize the residue and add one drop of safranin-o stain. Vortex mix again to mix the stain fully. The purpose of the stain is to make thin specimens more visible under the microscope, but specimens should not be too heavily stained. They should be pink and translucent. If residue is too heavily stained, the stain can be removed by adding some dilute HCl (which immediately removes the stain, neutralizing with distilled water, and then staining again.

36. While the residue is in the centrifuge (step 35), disassemble the sieve, rinse with distilled water to remove any remaining residue, and reassemble the sieve using the same sieving material. Clean the inside of the sieve material with a jet of distilled water from the squeeze bottle. This will clear any blocked pores and make the next sieving more efficient.

37. Transfer the stained residue from the 15 mL tube to the sieve holder and sieve as before. This step both washes out stain in the supernatant and gives the residue a final clean (absolutely necessary if the residue has undergone ultrasound treatment). After sieving, return the stained residue to the 15 mL tube and spin down in the centrifuge. Pipette off the supernatant until within about 3 or 4 mL and homogenize with the pipette. If the residue is too concentrated, then add some distilled water. The residue is now ready for slide making.

38. Prepare for slide making. About 10 mins before slide making, switch on covered slide warmer and hot plate for warming glycerine jelly. The slide warmer needs to be covered because the slides will be drying on it for ~1 hour and could otherwise collect airborne dust). Clean surface of covered slide warmer (slide drying bench) with damp kitchen toweling. Using a cleaned spatula, add around 10 mL of glycerine jelly (Appendix 1) to a 50 mL glass, round-bottomed centrifuge tube. Add a clean pipette, clearly marked at the top with a felt-tipped marker so it cannot be confused with a sample pipette. Wrap parafilm around top of centrifuge tube and pipette, to prevent dust from entering the glycerine jelly and to prevent excessive loss of water. Place this centrifuge tube in a 400 mL Pyrex beaker half-filled with hot water, and stand the beaker on hotplate at low heat. The temperature should be sufficient to keep the glycerine jelly

melted, but not much warmer. If the hotplate is too hot at its lowest heat, then place some microscope slides between the beaker and the base of the heater.

Fill a one-dram screw-top vial with distilled water. Have ready a box of cover slips and a box of wooden cocktail sticks (longer than tooth picks).

39. Place a cover slip on the slide warmer, and using a pipette add 2 drops of glycerine jelly and 6 drops of distilled water (from the vial prepared earlier). Mix using a cocktail stick. Make sure to cover all the cover slip's surface with the mix, taking advantage of the surface tension effects of the edges of the coverslip. If the glycerine jelly spills over, then discard, wipe up and start over again.

Then use a pipette to mix the sieved residue thoroughly, and promptly transfer about 10 drops of residue evenly over the cover slip. We usually prepare two cover slips in this way for each sample. Then lower the cover the slide warmer and let the cover slip dry for at least an hour. We use prewashed 22 x 40 mm cover slips.

40. Ensure that all superfluous water has evaporated from the cover slip. This can be done by placing a cold microscope slide over the cover slip to check for condensation. Put approximately 12 drops of glycerine jelly on a microscope slide and carefully invert the cover slip onto the glycerine jelly, avoiding any air bubbles from becoming trapped. Lower the coverslip slowly, and avoid dropping as this will very likely produce air bubbles. Then remove the microscope slide quickly from the slide warmer and let it rest horizontally for a few hours. This quick cooling prevents the glycerine jelly adhering the residue to the coverslip from melting and causing the

residue to sink. The purpose of this method is to have the residue on a single plane coincident with the base of the coverslip. The remaining glycerine jelly below the residue will ensure that the microscope slide never dries out. Slide-making follows the methodology of Evitt (1984).

41. When it is decided that no further slides will be made at this time, then the sieved and unsieved residues need to be stored permanently. We use 1 dram clear glass screw-top glass vials for the sieved residue and 2 dram vials for the unsieved residues, where 1 dram = 1/8 fluid ounce = ~3.7 mL (drams/fluid ounces are Imperial measures used in the US. Of course a 4 mL vial would work fine). Label the vials (lab number and some specific processing info. such as "10 µm, 30 secs u/s") and rinse with distilled water. Pipette the residue from the 15 mL (sieved) and 50 mL (unsieved) centrifuge tubes, into the 1 and 2 dram vials respectively. Leave to settle overnight.

The next day, pipette off the supernatant carefully to avoid disturbing any residue. Add glycerine from a dropper bottle until the vial is ~5/6th full. Add one drop of thymol/ethanol to the 1 dram vial and 2 drops to the 2 dram vial (Appendix 2). Close firmly with screw top, and shake vigorously to mix the residue, glycerine and thymol together. The vials can now be placed in long-term storage at room-temperature without drying out or the risk of microbial growth.

42. Residues stored in glycerine jelly (step 40) can be reconstituted by washing into a sieve with warm distilled water. They are then ready for making more microscope slides.

Mixing glycerine jelly

We use a modification of the original recipe from Kaiser (1880). The aim is to use jelly that is not too sticky and with too little shear strength (caused by too much glycerine) but with enough glycerine that will prevent the slides from eventually drying out (over time the gelatin will otherwise revert to a crystalline powder and the slide will be unusable and unable to be resuscitated).

Our gelatin has the brand name Knox gelatin (www.knoxgelatine.com/) and is used in cooking and baking. Be sure to use the colourless, unflavoured kind. Boxes of Knox gelatin contain pouches of 8 grams. Place one pouch (8 grams) with ~100–150 ml of distilled water into a clean Pyrex beaker. Add a stirring flea and place on a magnetic stirrer/heater. The gelatin dissolves faster with low heat (it must not boil as this would prevent thorough mixing). Cover with parafilm and allow to mix for about two hours. A smooth liquid should result. Add a little more water if the liquid is too thick. Then add 100 ml of glycerine and about 5 drops of allylphenol (we now use thymol). Mix and heat on the magnetic stirrer/heater for about 15 minutes. Pour the mixture into screw-top containers and allow to cool. Our experience is that this will give the good results. However, when reheating the mixture before making slides, it is possible to fine-tune the viscosity of the mixture by adding water to make it more liquid or adding glycerine to make it more sticky. We usually make up the glycerine jelly in a 1L Pyrex beaker, using 3 pouches of gelatin 400 ml of distilled water, and then 300 ml of glycerine (plus 15 drops of thymol; Appendix 2). This gives enough glycerine jelly for years of use.

Mixing thymol

In the past we have used liquefied thymol to preserve residues, but phenol is extremely toxic. Therefore we now use thymol, which is still toxic but much less so. It is still necessary to use with gloves and treat with care. One issue with thymol is that it has very low solubility in water (0.9 g/L at 20°C) but is much more soluble in ethanol (1000 g/L). We therefore place about 1 cm of crystals of thymol in a dropper bottle and fill to ¾ level with ethanol. Leave overnight and the most of all of crystals will have dissolved. If all are dissolved add more crystals until you have a saturated solution. The thymol crystals can be added to the dropper bottle by placing them on aluminum foil which is folded to allow the crystals to slide into the bottle. Do this over the sink so any stray crystals can be washed away. Thymol is somewhat soluble in glycerine (1 part thymol, 120 parts glycerine), and ethanol is miscible in both water and glycerine, so the thymol–ethanol solution can be added both to water and glycerine.

Lycopodium tablets

Tablets containing known quantities of acetolysed Lycopodium clavatum spores are available through the Department of Geology, Lund University, Sweden. In 2019, batch 140119321 became available. Each batch has its own specified number of spores per tablet, so it is important always to note which batch of tablets is being used in the preparation. Details of earlier batches, along with other very useful information for palynologists, are given on the Canadian Association of Palynologists (CAP) website at:

https://capacp.wordpress.com/library-resources/equipment-lab-supplies/

The concentrations of dinocysts is calculated using the formula in Stockmarr (1971, Pollen et Spores 13, 615–621). Concentrations estimated in this way are meaningless without knowing the associated errors. Errors on the estimated concentrations are calculated using the formula in Maher (1981, Rev. Palaeobot. Palynol. 32, 153–191).